


Electrospray molecular dynamics simulations using an octree-based Coulomb interaction methodNeil A. Mehta and Deborah A. Levin
The University of Illinois Urbana-Champaign, IL 61801, USA (Received 16 November 2018; published 11 March 2019)

A new octree-based Coulomb interaction model is developed to model the electrospray of ionic liquids (ILs) in molecular dynamics. Using an octree-based method, Coulomb interactions are categorized as intra- and interleaf Coulomb interactions based on a criterion related to the Bjerrum length of the IL. The octree-based method is found capable of reproducing Coulomb energy in agreement with established and computationally more expensive models, such as the direct Coulomb and the damped shifted force (DSF) method in the absence of an external electric field. In the presence of an external electric field, the octree-based method produces distinctly different results compared to that obtained by the direct Coulomb method. The time required to form Taylor's cone was shorter for the octree method compared to the direct Coulomb approach. While no emission larger than monomers was observed from the direct Coulomb simulation, emission of larger species such as dimers and trimers was observed when the octree-based Coulomb interaction model was used. Furthermore, the octree-based model forms a smaller ion emission cone compared to that from the direct Coulomb method.

DOI: [10.1103/PhysRevE.99.033302](https://doi.org/10.1103/PhysRevE.99.033302)**I. INTRODUCTION**

Electrosprays have been used extensively in the field of microfabrication for controlled deposition [1], in particular, microfilm deposition [2], microcircuit manufacturing [3], and ion-beam lithography [4]. More fundamentally, because of the ability to generate ions from macromolecules, electrosprays have been used to analyze the properties of ionic liquids (ILs) using electrospray ionization mass spectroscopy [5]. Similarly, the ability to generate energetic ionic emission has made it possible to use electrosprays with ILs as propellants to serve as a propulsion device for nanosatellite station keeping and microthrust adjustments [6–9]. The electrospraying process starts with the formation of a Taylor's cone [10], whereby a liquid surface deforms in the presence of high electric fields and ion clusters are then emitted from the tip of this cone toward the extractor ring. While traveling toward the extractor ring, the emitted ion clusters undergo further evolution due to the external electric fields. While electrosprays have been in use for more than 30 years, the underlying mechanism of cone formation and post emission droplet evolution at an atomistic level is only possible by performing molecular dynamics (MD) simulations [11,12].

From these simulations, it is understood that the process of electrospraying is primarily dominated by noncovalent forces and, in particular, contributions from the Coulomb interactions are key for any accurate MD simulations of electrosprays at the atomistic level. However, unlike van der Waals forces, Coulomb interactions decay as the inverse of interatomic radius, making these forces important over long distances and, therefore, computationally the most expensive part for MD simulations of charged systems. Traditionally, electrostatic interactions are divided between short and long ranges. Interactions are deemed short range if the interatomic distance is less than the user-defined cut-off radius. The short-range interactions are calculated using Coulomb's law while those over longer ranges are computed using long-range Coulomb interaction methods, such as the Ewald summation [13]. In

periodic charge dense systems, a cut-off radius of 10–15 Å is considered adequate to subdivide interactions into short and long ranges. However, for simulation domains with nanometer length scales, such as those used to model electrosprays, the spatial nonhomogeneity of ion-pair distributions lead to sparse charge regions which makes it necessary to use accurate long-range Coulomb models.

The choice of the long-range Coulomb model and the associated Coulomb cut-off radius significantly affects the outcome of MD electrospray simulations. From our previous electrospray MD simulations of 1-ethyl-3-methylimidazolium tetrafluoroborate (EMIM-BF₄), it was found that the accuracy of conventional long-range Coulomb interaction models strongly depend on the Coulomb cut-off radius and the domain size [12]. In that work, we found that previous electrospray MD simulations of coarse-grained EMIM-BF₄ [11] were performed using incorrect long-range Coulomb interaction parameters and the force-shifted Coulomb sum method [14]. This, in turn, led to a spurious weakening of Coulomb interactions and predicted abnormally high ion emissions.

Since MD simulations typically scale as $O(N^2)$, where N is the number of atoms used in the simulation, it is not feasible to use an infinitely large cut-off radius, as the simulations would become prohibitively expensive. We face a twofold problem of performing simulations with a cut-off radius small enough to keep the computation cost low for the short-range Coulomb interactions as well as having an accurate long-range model appropriate for the given MD simulations. For large simulations (> 10 000 atoms), the cut-off radius required to achieve convergence in the system's Coulomb energy also increases. There are a number of methods available to calculate the long-range part of electrostatic interactions that vary in their complexity of implementation. However, many of these methods require the domain to be periodic in all three dimensions to work efficiently. While long-range methods, such as particle-particle particle-mesh [15] methods have been reliable in MD simulations of bulk ionic liquids with

periodicity in at least two dimensions, they are found to be inaccurate for simulations with domains that have sparse density distributions, nonperiodicity, and charge nonhomogeneity in domains with high aspect ratios [12]. For these reasons, we propose a novel Coulomb interaction model based on the Barnes-Hut algorithm [16] to simulate such systems.

Hierarchical algorithms, such as the Barnes-Hut algorithm [17] and the fast multipole method (FMM) [18] have been used to compute Coulomb forces in MD simulations [19,20]. The standard steps involved in these algorithms are the construction of an octree structure, traversing the octree from the leaves to the root to calculate the Coulomb energies of atoms in each leaf due to atoms belonging to other leaves (outer expansion), traversing the octree from the root to leaves to calculate Coulomb energies inside the leaf due to atoms outside the leaf (inner expansion), which is then followed by the accumulation of forces on each particle. To access the parent-child information between leaves at the multiple levels of the octree, point-based octree approaches have been implemented. The need to have a pointer-based approach, however, makes FMM challenging to implement and its efficiency depends on how the particles are distributed in the domain [21]. Furthermore, the accuracy of the FMM method depends on the order of expansion. For astrophysical applications, which is one of the main areas of use, three expansion coefficients are considered adequate since they provide approximately three significant digits of accuracy [22]. For MD simulations, typically, five digits of accuracy are needed, which is possible only when seven expansion coefficients are used [23]. Although considerable work has been done to parallelize the FMM method on computers with distributed memory with good efficiency [24–27], it generally scales poorly with increasing number of processors for expansion coefficients greater than three. To circumvent problems associated with pointer-based octree methods, we present a Barnes-Hut-based algorithm, which relies on a linearized octree structure [28], similarly to the approach used by Jambunathan and Levin [29] for their work on particle-in-cell methods. The linearization of the octree makes it possible to implement this method with the existing LAMMPS framework [30].

We present here a Barnes-Hut-based Coulomb interaction model with the specific intent of studying the evolution of ionic liquid systems with a nonhomogeneous charge distribution in the domain. In this work, we perform all-atom MD simulations of ethylammonium nitrate (EAN) using the new Coulomb interaction method. EAN is categorized as a room-temperature ionic liquid and is one of the oldest-known ILs [32] with the chemical structure and atomic partial charge shown in Fig. 1. The electrochemical properties of EAN have been analyzed in detail using both experiments [33] and MD simulations [31,34,35]. Lenguito *et al.* [36] and Alonso-Matilla *et al.* [37] have experimentally shown that EAN can be successfully electrospayed.

To demonstrate the capability of the octree-based Coulomb interaction model, two categories of simulations have been performed. The first set of simulations are used to study the fluctuations and energy stability of the octree-based method during the evolution of an isolated droplet of EAN. In the second set of simulations, the extrusion of EAN is simulated using a larger domain to model the entire electrospay process,

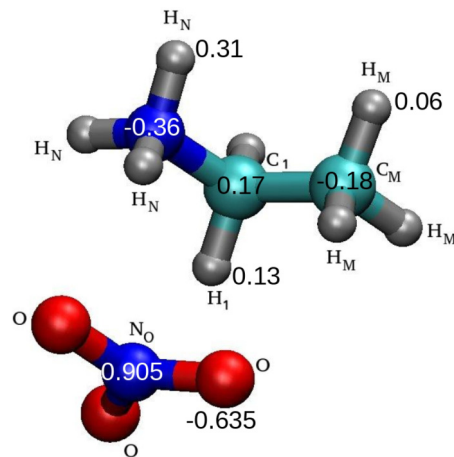


FIG. 1. Molecular structure and atom types of EAN. Subscripts are used to differentiate the carbon and hydrogen atoms based on their position in the molecular skeleton [31]. Atom colors are as follows: C (teal), H (silver), N (blue), and O (red). The EAN molecule is approximately 5.0 Å across in dimension. Partial charge on each atom is as labeled.

including the initial time-steps when the Taylor’s cone is formed. To validate the Coulomb energies and total energy predicted from the octree-based Coulomb interaction model, the same set of simulations have also been performed using Coulomb’s law directly, but with a large cut-off radius of 40 Å. We discuss the improvement in accuracy when the octree-based method is used and look at the differences in the Coulomb energy and emission species and currents that result from these two methods.

II. NUMERICAL FRAMEWORK FOR THE OCTREE-BASED COULOMB MODEL

To improve computational efficiency without compromising the accuracy of the Coulomb energy, an octree-based Coulomb interaction model is proposed to calculate the short- and long-range Coulomb energies. An octree is a hierarchical structure which encompasses a domain that will undergo recursive subdivision into eight equal parts until a user-defined criterion is satisfied. In this structure, the three-dimensional simulation domain encompassing all the atoms in the system forms the first internal node, also known as the root or the queen. The root is divided into octants or children, which are the first generation of nodes. Based on the two limiting criteria, namely (1) the number of particles present in the children and (2) its dimension, the children nodes will undergo further recursive subdivision, until one of the two conditions are met. The final nodes that do not undergo subdivision are known as the leaf nodes. Note that a leaf is analogous to a cell in grid-based methods. A schematic of a two-dimensional octree is shown using arbitrary notional particles, representing the partial charges, instead of actual ion pairs for simplicity, in Fig. 2(a). The red outermost frame, which encompasses the domain is known as the root of this octree. During the MD simulation, the root then undergoes recursive subdivision, every time step, to form leaves, which are analogous to cells of a uniform grid. In this example, the octree root has 10 leaves.

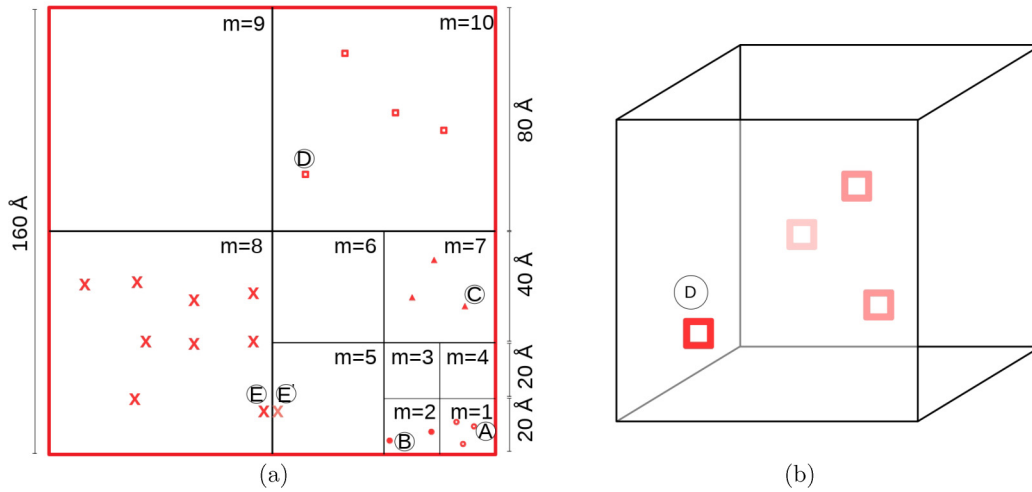


FIG. 2. Example of an arbitrary octree structure constructed with $R_{\text{inner}} = 20 \text{ \AA}$; particles A–E denote notional ion pairs. Figure on the right shows a three-dimensional view of the octree leaf ($m = 10$).

The electrostatic interaction energy between the partial charges of atoms i and j is given by Coulomb’s law as

$$\mathcal{A}_{ij} = C \frac{q_i q_j}{r_{ij}}, \quad (1)$$

where r_{ij} is the distance between atoms i and j , C is Coulomb’s constant, and q_i, q_j are the user-defined partial charges on atoms i and j , respectively, as shown in Fig. 1. For a group of n atoms, the Coulomb energy is given as

$$E_{\text{Coul}} = \sum_{i=1}^{n-1} \sum_{j=i+1}^n \mathcal{A}_{ij}. \quad (2)$$

These electrostatic interactions scale as $1/r$, which leads to large fluctuations in energy for small changes in r_{ij} at distance less than 15 \AA but the fluctuations decay rapidly over larger distances ($>60 \text{ \AA}$). When charge interactions are calculated by summing up the atomic partial charges over large interatomic distances, using Eq. (2) becomes computationally expensive. To overcome this limitation, the electrostatic energy calculations are split into short- and long-range Coulomb interactions, based on a user specified cut-off distance, R_c , and the electrostatic energy is now calculated as

$$E_{\text{Coul}} = E_{\text{short-range}} + E_{\text{long-range}}, \quad (3)$$

where the first term, $E_{\text{short-range}}$, takes into account all interactions with radius less than R_c and is commonly known as E_{direct} [38],

$$E_{\text{short-range}} = E_{\text{direct}} = \sum_{i=1}^{n-1} \sum_{j=i+1}^n \mathcal{A}_{ij} \quad \text{for } r_{ij} < R_c. \quad (4)$$

$$\begin{aligned} B_{ij} = C\kappa \left\{ \frac{\text{erfc}(\alpha_d \chi)}{\chi} - \frac{\text{erfc}(\alpha_d R_S)}{R_S} \right. \\ \left. + \left[\frac{\text{erfc}(\alpha_d R_S)}{R_S^2} + \frac{2\alpha_d}{\sqrt{\pi} \frac{\exp(-\alpha_d^2 R_S^2)}{R_S}} \right] \right. \\ \left. \times (\chi - R_S) \right\} \quad \text{for } \chi \leq R_S. \quad (5) \end{aligned}$$

Using Eq. (2) with a cut-off radius leads to a major drawback, because the charges contained within the cut-off radius must be charge neutral. However, as the atomic partial charges move back and forth across the cut-off radius in subsequent time steps due to fluctuations in interatomic forces, the region inside the cut-off radius is no longer charge neutral and can cause a kinetic energy drift or a spurious energy gain within the system. Also the Coulomb energy calculations are no longer be considered “stable” or energy conserved [39]. These fluctuations in the interatomic forces are inherent to all MD simulations and one way of addressing them is by shifting and dampening the Coulomb interactions, such that they are close to zero at the cut-off radius. Using the damped shifted force (DSF) method of Fennell and Gezelter [14], the \mathcal{A}_{ij} term in Eq. (2) can be modified by introducing the shift radius, R_S , and dampening parameter, α_d , as shown in Eq. (5), where, $\kappa = q_i q_j$ and $\chi = r_{ij}$. The complementary error function, erfc , is introduced to reproduce the effective screening used by the Ewald summation method and the dampening parameter accelerates the convergence of the Coulomb energies by dampening the Coulomb energy fluctuations around the shift radius [40,41]. It can be observed that Eq. (5) will simplify to Eq. (2) if the dampening parameter, $\alpha_d = 0$ and shift radius, R_S tends to infinity. The R_S and α_d parameters are interdependent and the choice of R_S used for the simulations of this work will be discussed in Sec. III. Equation (5) has been specifically used to obtain Coulomb energies for charged systems in a continuous bulk media. Typically, for simulations of bulk media, a smaller shift radius, and, consequently, a larger dampening parameter, is adequate as there are sufficient charges that contribute to the Coulomb energy within the spherical volume of radius equal to the shift radius. However, simulations of electrospays represent a domain with nonhomogeneous, sparsely distributed charges which will require very large ($>160 \text{ \AA}$) shift radius and a small dampening parameter to accurately account for charges distributed over longer ranges. Since a larger shift radius could negate the benefits obtained by using Eq. (5), some modification of the DSF method will be required for the octree-based method.

For the octree-based Coulomb interaction method, the Coulomb interactions are divided into the intra- and interleaf Coulomb energies,

$$E_{\text{Coul}} = E_{\text{intraleaf}} + E_{\text{interleaf}}, \quad (6)$$

where $E_{\text{intraleaf}}$ is calculated as the sum of Coulomb interactions between all particles belonging to that octree leaf using

$$E_{\text{intraleaf}} = \sum_{m=1}^l \sum_{i=1}^{n_m-1} \sum_{j=i+1}^{n_m} \mathcal{B}_{i,m;j,m}, \quad (7)$$

where l is the total number of leaves in the octree, n_m is the number of atomic partial charges in octree leaf m . For the schematic of an octree shown in Fig. 2(a), the intraleaf Coulomb interactions are evaluated using Eq. (7) over all 10 leaves. Figure 2(b) shows that the $E_{\text{intraleaf}}$ contribution from leaf $m = 10$ will have Coulomb interactions from only the four notional particles belonging to that leaf.

To compute the $E_{\text{interleaf}}$ term, which includes the Coulomb interactions between atomic partial charges belonging to different leaves, the center of mass of each leaf, \vec{R}_p , is first calculated and assigned a charge equivalent to the sum of charges of all particles belonging to that leaf, i.e.,

$$\vec{R}_p = \frac{\sum_{i=1}^{n_p} m_{i,p} \vec{r}_{i,p}}{\sum_{i=1}^{n_p} m_{i,p}}, \quad (8)$$

where p is the leaf index, n_p is the total number of atoms belonging to leaf p , and $\vec{r}_{i,p}$ and $m_{i,p}$ are the position vector and mass of the i th particle belonging to leaf p , respectively. The charge, Q_p , associated with the leaf p is calculated as

$$Q_p = \sum_{i=1}^{n_p} q_{i,p}. \quad (9)$$

The interleaf Coulomb energy is then calculated using

$$E_{\text{interleaf}} = \sum_{m=1}^{l-1} \sum_{p=m+1}^l \begin{cases} \sum_{i=1}^{n_m} \sum_{j=1}^{n_p} \mathcal{B}_{i,m;j,p} & \text{for} \\ r_{i,p} \leq R_{\text{inner}}\theta, \\ \sum_{i=1}^{n_m} \mathcal{B}_{i,m;p} & \text{for} \\ r_{i,p} > R_{\text{inner}}\theta \end{cases}, \quad (10)$$

where, for $\mathcal{B}_{i,m;p}$, κ is now calculated as the product of $q_{i,m}$ and Q_p , $\chi = |\vec{r}_i - \vec{R}_p|$ is the distance between the i th atomic partial charge belonging to leaf m and the center of mass of leaf p . Note that the intra- and interleaf energy terms are analogous to the conventionally used terminologies of the short- and long-range interactions but with some important differences. In the octree-based Coulomb method, the short-range Coulomb interactions are now calculated using the intraleaf term by Eq. (7) and the first part of the interleaf term of Eq. (10).

The demarcation between the short- and long-range Coulomb interactions, R_{inner} and θ , is not decided arbitrarily using a Coulomb cut-off radius. The inner radius, R_{inner} , corresponds to the dimensions of the smallest leaves in the octree and the accuracy parameter, θ , determines the extent of the short-range Coulomb interaction. The product of the inner radius and the accuracy parameter becomes the effective cut-off radius over which Coulomb interactions are deemed

short range. For example, in the octree schematic constructed using the R_{inner} criterion of 20 Å, shown in Fig. 2(a), assuming that $\theta = 2$, the interoctree Coulomb energy between notional particles A and B is computed using the first row of Eq. (10), since the distance between notional particle A and the center of mass of leaf $m = 2$, which contains notional particle B, is less than $R_{\text{inner}}\theta$. The distances between notional particle A and the center of mass of leaves $m = 7, 8$, and 10 are greater than $R_{\text{inner}}\theta$. Therefore, to calculate the Coulomb interaction between notional particles A and C, D, E, the second row of Eq. (10) is used.

The schematic shown in Fig. 2(a), also explains the origin of fluctuations that will also be observed in energy conservation for the octree-based Coulomb interaction method. If we consider the interaction between notional particles B and E, where notional particle E lies at the boundary of leaves $m = 8$ and 5, then it is clear that, due to small fluctuations in its positions generated by interactions with other notional particles or kinetic energy, notional particle E may lie either in leaf $m = 7$ or 5 in subsequent time steps during the simulation. When notional particle E is present in leaf $m = 5$, its Coulomb interaction energy will be calculated using the first expression of Eq. (10) as the distance between the centers of mass of leaves $m = 2$ and 5 is less than $R_{\text{inner}}\theta$. However, when notional particle E jumps to leaf $m = 7$ in the next time step, the partial charge on notional particle E will now be approximated as a coarsened charge located at the center of mass of leaf $m = 7$ because the distance between the centers of mass of leaves $m = 2$ and 7 is greater than $R_{\text{inner}}\theta$. In the absence of dampening and force shifting, this would lead to differences in the Coulomb energy calculated in subsequent time steps that would cause a spurious gain in kinetic energy of the system.

The octree algorithm proposed by Barnes-Hut [16] does not specify a lower limit on the minimum dimensions of the leaf, R_{inner} , but instead requires that each octree leaf should not contain more than one particle. However, this approach would not be computationally practical in regions with high number densities of atoms or for accurately maintaining the long-range order of the liquid during the simulation. Therefore, the accuracy parameter, θ , and inner radius, R_{inner} , are selected based on physical considerations. For the ionic liquid simulations, we propose that R_{inner} must be adequately large to capture all the coordination shell radii or peaks of the radial density function (RDF) of the bulk IL system under consideration. The average location of individual ions in a bulk solution is expressed in terms of a radial density function, $g(r)$. This function represents the probability of finding another ion at a particular distance, r , from an individual ion. Similarly to the crystal structure of solids, there are distances at which ions can be found with a higher probability relative to other ions in ionic liquids. The distances at which a higher probability of ions is observed is unique to each ionic liquid and is referred to as the long-range order, which can be verified using x-ray diffraction studies and MD simulations. For the nitrogen atoms of the ammonia and nitrate groups, representing the cation and anion parts of EAN, it is observed that the long-range order or atom-atom correlation persists to approximately 12 Å, as shown in Fig. 3. Therefore, a value of $R_{\text{inner}} = 10$ Å is implemented as the smallest leaf size for

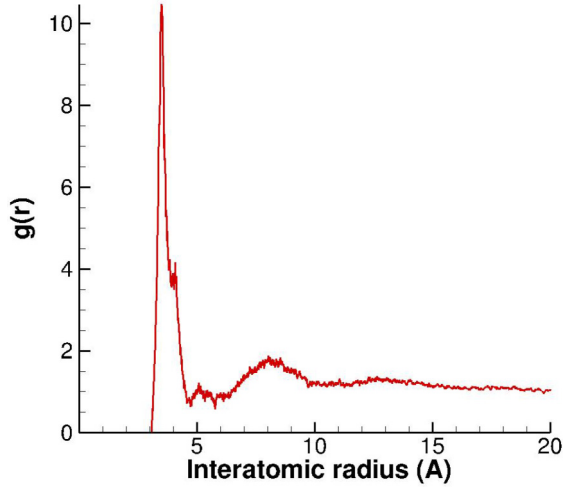


FIG. 3. Radial distribution function of ammonia and nitrate nitrogen atoms of EAN.

the octree-based Coulomb interaction model to perform MD simulations of EAN.

The Debye-Hückel-Bjerrum theory is used to obtain the accuracy parameter, θ , from the Bjerrum length, λ_B . The Bjerrum length is defined as the distance at which the electrostatic interaction between two ions of opposite charges is comparable in magnitude to thermal energy, $k_B T$, of the medium, which in our study is the energy equivalent to the temperature of the ionic liquid [42,43]. To obtain the Bjerrum length, we use the Poisson-Boltzmann equation and the number density of the medium, \tilde{n} to derive the inverse Debye screening length,

$$\kappa_0 = \sqrt{4\pi\lambda_B\tilde{n}(r)} = \sqrt{\frac{\tilde{n}(r)e^2}{\epsilon_0\epsilon_n k_B T}}, \quad (11)$$

such that the Bjerrum length, λ_B , is

$$\lambda_B = \frac{e^2}{4\pi\epsilon_0\epsilon_n k_B T}. \quad (12)$$

Using $\epsilon_n = 25.1$ as the dielectric constant [33], in Eq. (12), the Bjerrum length of EAN is calculated to be, $\lambda_B = 22.19$ Å. The Bjerrum length represents the distance over which the Coulomb interaction is significantly more important for a given charge dense system compared to contributions from covalent bonds, angles, dihedrals, van der Waals potential, and kinetic energy. Thus, a larger value of $R_{\text{inner}}\theta = 30$ Å is a reasonable criterion to demarcate the boundary between short- or long-range interactions for EAN simulations. Since the value of R_{inner} for EAN is 10 Å obtained from the radial density function, an accuracy parameter $\theta = 3$ is obtained. Using this hypothesis, we expect to obtain converged Coulomb energy values for the EAN simulations when using $R_{\text{inner}} = 10$ Å and $\theta = 3$, as will be demonstrated in Sec. III.

Finally, because the octree is an adaptive grid, the grid generation process is dynamic. During the MD simulations, the octree structure from the previous time step is destroyed and recreated every time step to ensure that the number of atomic partial charges in each leaf satisfy the recursive subdivision criterion at any given time. To construct the octree grid, the root is recursively subdivided using the R_{inner} and a

minimum number of particles criteria. First, the number of ion pairs (or partial atomic charges) in each leaf is counted. If there are more than two ion pairs (~ 40 atoms) inside a leaf, then that leaf is subdivided further. This process is performed until either the number of ion pairs in each leaf is a maximum of two or the leaf size is equal to $R_{\text{inner}} = 10$ Å. During the simulation, atomic partial charges move from one leaf to another, which may cause the number of atomic partial charges in a leaf to be higher than the criteria used for the recursive subdivision. This is not problematic when calculating intra-leaf Coulomb interactions using Eq. (7) because all atomic partial charges mapped to each leaf are considered. However, when additional atomic partial charges enter into a previously formed octree leaf, the center of mass, \vec{R}_p , calculated using Eq. (8), as well as the charge associated with that leaf, Q_p , are affected. During the interleaf Coulomb evaluations, changes in center of mass and charges associated to the leaves when the octree structure itself has not changed would result in Coulomb interactions being calculated using the second expression of Eq. (10) instead of the first, which may lead to a spurious gain in kinetic energy.

III. MD SIMULATION SET-UP AND VALIDATION OF OCTREE-BASED COULOMB INTERACTION MODEL

To validate and assess the accuracy and efficiency of the octree-based Coulomb interaction method, two sets of MD simulations of EAN were performed using both direct Coulomb as well as the octree-based Coulomb interaction models. Since the EAN molecule consists of a relatively small cation and anion species, compared to more complex aprotic and other protic ILs, it is a good candidate to study the effects of Coulomb interaction models in the presence of an external electric field. For the simulations discussed in this section, 2000 ion pairs of EAN were arranged in a spherical geometry, with an approximate radius of 40.81 Å. The primary droplet, for this case, represents a large droplet that could be emitted in an electrospray and is large enough to analyze the effects of the Coulomb model but is also computationally tractable. The spherical arrangement of EAN ion pairs is henceforth referred to as the primary droplet to distinguish it from the secondary emissions that occur when a droplet is placed in the presence of an external electric field. The primary droplet was placed in the center of the simulation domain with dimensions $160 \times 160 \times 1280$ Å. However, since it is necessary to have a cubic domain shape to generate the octree root, the simulation domain was divided into eight equal roots, each of size $160 \times 160 \times 160$ Å. Initially, the ion pairs were arranged randomly within a sphere, which was followed by potential energy minimization step to eliminate unrealistic ion arrangements and atom-bond overlaps generated while arranging the ion pairs. A canonical ensemble (NVT) simulation was performed for 250 ps using the Berendsen thermostat to lower and maintain the EAN primary droplet at 5.0 K.

All MD simulations in this work were performed using the LAMMPS toolkit [30]. The optimized potential for liquid simulations all-atom (OPLS-AA) interatomic potential used for the EAN simulations was obtained from the work of Jorgensen, *et al.* [44] and Umebayashi, *et al.* [34]. A cut-off radius of 12.0 Å was used for the Lennard-Jones forces

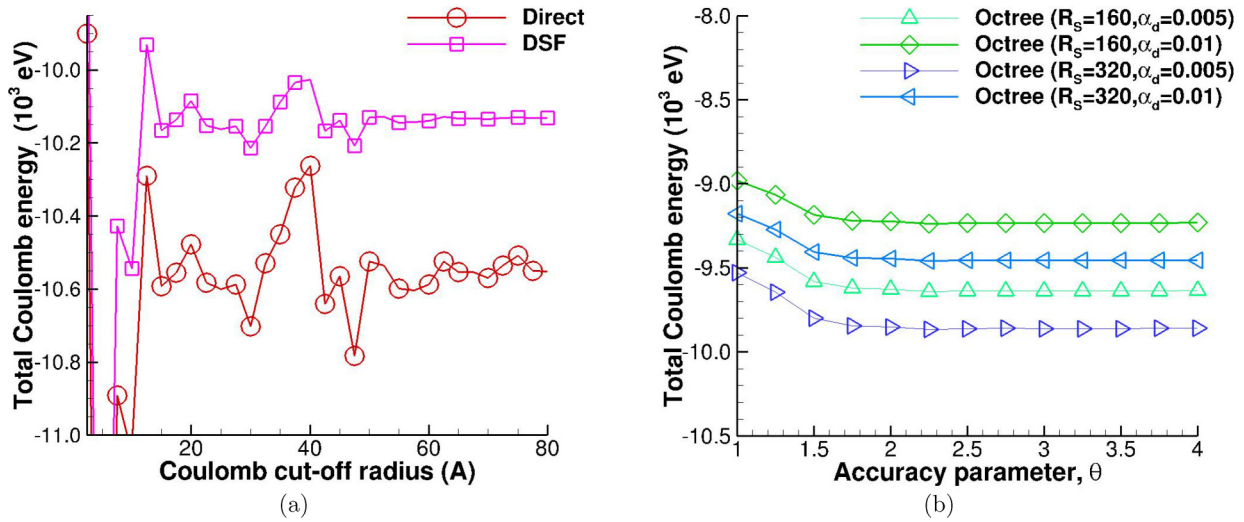


FIG. 4. Comparison of Coulomb energy convergence for a single snapshot taken at a time of 35 ps of atom positions of 2000 ion pairs representing a EAN primary droplet at a temperature of 5.0 K. Direct Coulomb and DSF method ($R_S = 320$ Å, $\alpha_d = 0.005$) comparison shown in the left panel and octree-based Coulomb interaction method shown in the right.

between the atoms. Each EAN ion pair was modeled using nine covalent bonds and angles simulated using harmonic potentials. Each ion pair was also modeled with four dihedral angles simulated using the OPLS potential. The covalent and noncovalent interaction parameters used in this work are provided as supplementary materials. A time-step value of 0.5 fs was used for all the simulations. In addition to the octree-based Coulomb interaction method, all direct Coulomb and DSF simulations of the primary droplet were performed using a Coulomb cut-off radius of 40 Å. Note that a Coulomb cut-off radius of this size is not possible in the larger electro spray simulations performed in the presence of an external electric field that will be discussed in Sec. IV. Therefore for those larger simulations, the Coulomb cut-off radius will be reduced to 20 Å.

A. Selection of octree-based Coulomb interaction model parameters

There are three independent variables, namely R_S , R_{inner} , and α_d , that are needed in the MD simulations with the octree-based Coulomb interaction model. To understand the sensitivity of the MD simulations to these parameters, the direct Coulomb method [Eq. (4)], the DSF method [Eq. (5)], and the octree-based Coulomb method [Eqs. (7) and (10)] were used to calculate the Coulomb energy of a single snapshot composed of 2000 ion-pair EAN droplets held at 5.0 K, as a function of the aforementioned parameters. Wolf, *et al.* [39,45] and Demontis, *et al.* [46], recommend that the shift radius used in the MD simulations should be $R_S \geq 5d_{ij}$, where d_{ij} is the distance between the cation and anion in the first coordination shell. From the radial distribution function of the nitrogen atom of the ammonia and nitrate groups of EAN, shown in Fig. 3, the first coordinate shell radius is $d_{ij} = 4.0$ Å, which leads to an $R_S = 20$ Å. Demontis *et al.* [46] also suggest that the optimal dampening parameter should be $\alpha_d = 2/R_S$. These recommendations for R_S and α_d were made for MD simulations of systems of 432 MgO molecules

and aluminosilicate-water, respectively. These, however, are not adequate for MD simulations of ILs because the long-range order in liquids extends to longer distances compared to solids. Furthermore, as stated previously, when force shifting is used, all interactions beyond R_S are ignored. Therefore, for the octree-based method, a larger shift radius is used. The purpose of using the octree-based method is to account for Coulomb interactions over distances greater than 60 Å and a smaller shift radius would not allow us to account for these interactions. Since the EAN primary droplet has a diameter of 80 Å, a shift radii of 160 (two times the diameter) and 320 Å (four times the diameter) are used in the MD simulations. Using the expression given by Demontis *et al.* [46], the associated α_d values for $R_S = 160$ and 320 Å are 0.01 and 0.005, respectively.

The comparison of the system Coulomb energy obtained from different Coulomb models is shown in Fig. 4. As shown in Fig. 4(a), using the dampening and force shifting for the DSF method with $R_S = 320$ Å and $\alpha_d = 0.005$ leads to a reduction (less negative) in the Coulomb energy of the system due to charge-screening and dampening of the Coulomb energies compared to that obtained from the DC method. When the DC or DSF method is used, it generates large fluctuations in Coulomb energies for small changes in the cut-off radius and provides converged results only beyond large cut-off distances greater than 40 Å. In comparison, as shown in Fig. 4(b), the octree-based Coulomb interaction model implemented using Eqs. (7) and (10) provides converged (nonfluctuating) Coulomb energy for an accuracy parameter as small as $\theta = 1.75$ ($R_{\text{inner}}\theta = 17.5$ Å) for all the selected R_S and α_d values but due the dampening and shifting, the Coulomb energies are lower (less negative) than that from the direct method. The octree-based method allows one to account for electrostatic contributions over distances greater than traditional cut-off radii used for the DC method, which leads to better convergence when calculating the Coulomb energy. It is observed that decreasing the shift radius or increasing the dampening parameter leads to lower (less negative) Coulomb

energy indicating a weakening of cohesion of the droplet structure. The Coulomb energy calculated by the DSF and the octree-based method with $R_S = 320 \text{ \AA}$ and $\alpha_d = 0.005$ are in close agreement and therefore these R_S and α_d values will be considered as the baseline values.

B. Validation of energy conservation using droplet simulations

For MD simulations of charge dense systems, it is vital to ensure that the selected Coulomb interaction method does not introduce large, spurious energy gains in the system due to numerical artifacts. One method of testing the presence of spurious energy gains is to perform microcanonical ensemble or constant number of particles, volume, and energy in the system (NVE) MD simulations of charged systems using different Coulomb interaction methods, during which the potential and kinetic energy of the atoms are monitored. As mentioned previously, while the use of any limiting cut-off condition in treating Coulomb interactions precludes strict energy conservation, the gain or loss of energy should be small ($<1\%$) in comparison to the sum of the kinetic and potential energies. To test the energy conservation of the octree-based Coulomb interaction model, the primary droplet maintained at 5.0 K is simulated for an additional 25 ps using the Berendsen thermostat, following which the thermostats are removed. The droplet is then simulated using a microcanonical ensemble (NVE), where any spurious changes of kinetic or potential energy are monitored. The primary droplet at 5.0 K has intentionally very low kinetic energy so that even small gains in energy can be easily observed. At higher temperatures, the gain in the kinetic energy would be a very small fraction of the total energy and would only be detected after considerably longer simulation time compared to that required for a 5.0 K primary droplet simulation.

When the Coulomb energy from the nondamped and non-shifted octree-based Coulomb model ($R_S = \infty$, $\alpha_d = 0.0$) is compared with that obtained for the direct Coulomb method using $R_c = 40 \text{ \AA}$ [Eq. (4)], large differences are observed in the potential energy, as shown in Fig. 5(a). In the presence of a thermostat, during the NVT phase of the simulation, the Coulomb energies from the nondamped octree-based and direct method agree within 1.0% ($-10\,400 \text{ eV}$ versus $-10\,300 \text{ eV}$, respectively). However, in the absence of a thermostat for the nondamped octree-based simulation, the thermal motion of the atoms, back and forth across the leaf boundaries at distances equal to the effective cut-off radius ($R_{\text{inner}}\theta$) leads to large gain in kinetic energy of the atoms, which is then reflected by an increase in the Coulomb energies in the subsequent time steps, as shown in Fig. 5(a). A similar analysis of the isolated primary droplet is also performed using the DSF method [Eq. (5)] with a shift radius of $R_S = 320 \text{ \AA}$, and the dampening parameter, $\alpha_d = 0.005$. It is observed from Fig. 5(a) that the Coulomb energy obtained from the DSF method is 3.0% lower than that obtained from the direct method at all simulation times ($-10\,050 \text{ eV}$ versus $-10\,300 \text{ eV}$, respectively). Another noticeable difference between the two methods is reduced fluctuations in the calculated Coulomb energy of the system when the DSF method is used compared to the direct method. Shifting the potential truncates the electrostatic interactions and neglects

all interactions beyond the shift radius. However, because the shift radius of 320 \AA is sufficiently large to encompass the entire droplet geometry, the effects of this shift are minimal. In parallel, as discussed previously, the use of dampening parameter allows charge screening at the shift radius, reducing the influence of atoms moving back and forth at this radius. This leads to lower Coulomb energy fluctuations in the DSF Coulomb energies shown in Fig. 5(a).

Because shifting and dampening are also used in the octree-based method, the results from the DSF simulations are used as the baseline for comparison. The octree-based Coulomb model [Eqs. (7) and (10)] is used to perform simulations for different combinations of R_S and α_d . From Fig. 5(b), it can be observed that using the octree-based method with shift radius and dampening parameter eliminates the spurious gain previously observed for the non-damped octree-based case shown in Fig. 5(a). Furthermore, compared to the Coulomb energies obtained from DSF method, the octree-based method results are free of fluctuations. For the DSF and octree-based simulations performed using the same $R_S = 320 \text{ \AA}$ and $\alpha_d = 0.005$, the Coulomb energies from the octree method is only 1.0 % lower than those obtained from the DSF case (-9950 eV versus $-10\,050 \text{ eV}$). When the DSF method is used, all Coulomb interactions within the shift radius are treated using Eq. (5). But when the octree-based Coulomb interaction method is used, interactions between atomic partial charges for distances greater than the $R_{\text{inner}}\theta$ criterion are computed using the center of mass of the leaf and its associated charge [second part of Eq. (10)]. This coarsening of charges allows computational saving albeit with a small loss of accuracy, as indicated by a relative difference of only 1.0% in the computed Coulomb energies. As previously discussed in Sec. III, the recommended dampening parameters for shift radii of 160 and 320 \AA are 0.01 and 0.005, respectively. However, to analyze the effect of varying the dampening parameter, simulations are also performed using $R_S = 160 \text{ \AA}$ with $\alpha_d = 0.005$ as well as using $R_S = 320 \text{ \AA}$ and a $\alpha_d = 0.01$. It was found that using a larger dampening parameter or decreasing the shift radius adversely affects the calculation of Coulomb interactions by weakening the Coulomb energies of the system, as shown in Fig. 5(b).

A comparison of the total (sum of potential and kinetic) energy of the system for these simulations are shown in Figs. 5(c) and 5(d). As shown in Fig. 5(c), while the total energy from the direct and DSF simulations remain steady, the nondamped octree-based simulation shows a significant increase in the total energy. Since the Coulomb energy is the dominant contributor to the potential energy, the rise of the total energy for the nondamped octree-based method shown in Fig. 5(c) compared with that from the Coulomb energy in Fig. 5(a) 25 ps onward shows that the total energy increases more rapidly than the Coulomb energy. This indicates that the kinetic energy of the system increases more rapidly than the Coulomb energy. This rapid increase of kinetic energy suggests that even small changes in Coulomb energy will lead to a large increase in the kinetic energy of the system. Although the total energy obtained using the DSF and octree method with $R_S = 320 \text{ \AA}$ and $\alpha_d = 0.005$ can be seen in Fig. 5(b) to be in agreement, the octree-based method shows

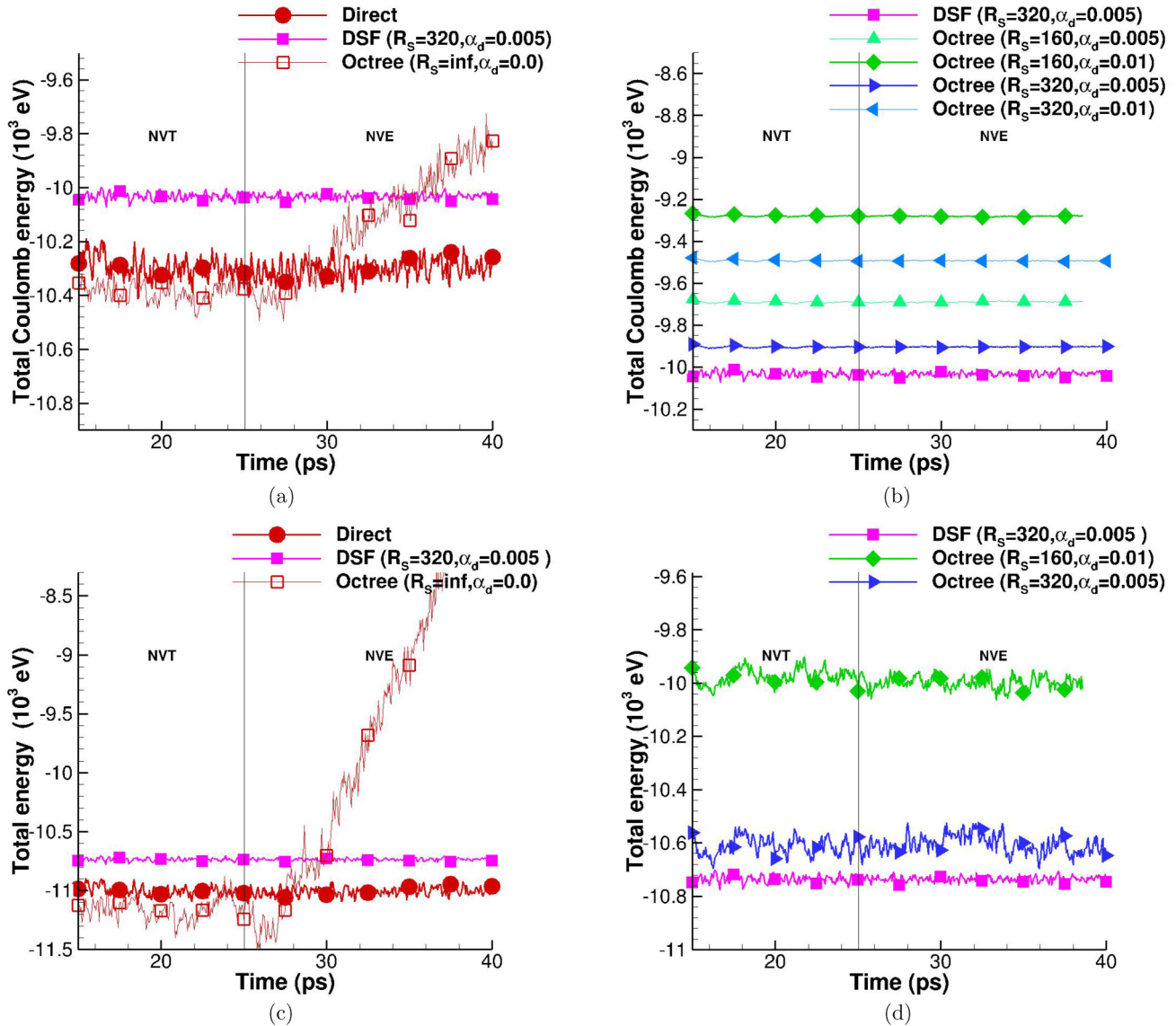


FIG. 5. Comparison of Coulomb energy and total (potential + kinetic) energy of an isolated primary droplet. Coulomb energy calculated using direct [Eq. (4)], DSF [Eq. (5)], and octree-based method [Eqs. (7) and (10) with $R_S = \infty$ and $\alpha_d = 0.0$] shown in (a). Coulomb energy calculated using DSF and octree-based methods [Eqs. (7) and (10)] shown in (b). Total energy of simulations using direct, DSF, and octree-based method ($R_S = \infty$ and $\alpha_d = 0.0$) shown in (c). Total energy of simulations using octree-based methods shown in (d).

comparatively higher fluctuations in total energy. While the Coulomb energy obtained using the octree-based method, as shown in Fig. 5(b), is comparatively smoother compared to the DSF method because of the coarsening of charges beyond $R_{\text{inner}}\theta$, coarsening also leads to loss of accuracy in calculating the electrostatic potential between any two particles at these distances. Considering the example octree shown in Fig. 2(a), there is a small difference in the electrostatic potential energy generated on particle D due to particle A, which is not equal to that generated on particle A by particle D due to the use of coarsening. However, it should be noted that over multiple time steps these small difference are canceled out resulting in a steady Coulomb energy calculations, devoid of spurious gains, as shown in Fig. 5(d). Consistent with the lower Coulomb energy (less negative) calculated using the octree-based method for $R_S = 160$ and $\alpha_d = 0.01$, the total energy calculated for this simulation is also lower (less

negative) compared to the DSF and the nondamped octree-based simulation.

Even though there are differences in the Coulomb energy of the system when either the Coulomb model or the model parameters are changed, the RDFs of the ammonia and nitrate nitrogen atoms for the DSF and the octree-based methods were found to coincide. The coordinate shell locations and their intensities obtained from all Coulomb models were the same, which suggests that the RDF and, as a consequence, the EAN mass density are not affected by the shift radii and dampening parameters used in this work.

C. Energy fluctuations due to leaf jumping

The octree-based Coulomb interaction method must ensure the continuity of the Coulomb forces across the interface between the intra- and interleaf Coulomb interaction limits.

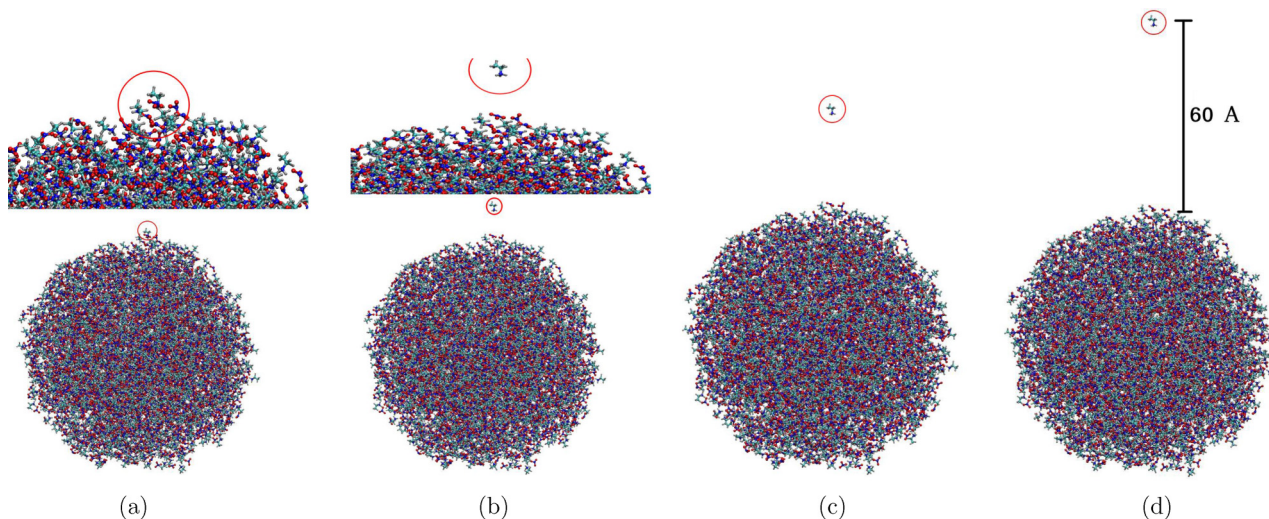


FIG. 6. Snapshots of the simulation with constrained cation moving away from the primary droplet surface. Distance between cation and the droplet surface in (a), (b), (c), (d) is 0, 10, 30, and 60 Å, respectively.

This is tested by artificially moving a single cation away from the primary droplet surface. The cation is moved 0.1 Å every time step and the simulation is stopped when the cation moves 100 Å from the primary droplet surface. Snapshots from this MD simulation are shown in Fig. 6. When the cation is at the primary droplet surface or 10 Å above it, as shown in Figs. 6(a) and 6(b), respectively, the cation is acted on by the Coulomb interaction from half the primary droplet using Eq. (7) because the effective cut-off is $R_{\text{inner}}\theta = 30$ Å. When it is moved farther than 30 Å away from the droplet surface, as shown in Figs. 6(c) and 6(d), the Coulomb interactions of the ion with the droplet are calculated entirely using Eq. (10).

The Coulomb energy of the cation during its motion away from the droplet should be devoid of spurious gains or losses within reasonable limits. As the cation moves away from

the droplet, the Coulomb energies generated between the cation and the droplet by the direct and DSF methods are in reasonable agreement, as shown in Fig. 7(a). The nonhomogeneous distribution of atomic partial charges inside the primary droplet as the cation moves away leads to fluctuations in the Coulomb energy. For the DSF method, the electrostatic interactions between the atoms of the cation and the rest of the primary droplet are calculated on a per-atom basis, whereas, for the octree-based method, the interactions between the cation and the primary droplet ion pairs are evaluated as a combination of intraleaf (within the $R_{\text{inner}}\theta$ limit) and by using the center-of-mass weighted average of charges (beyond $R_{\text{inner}}\theta$ distance). This leads to lower (less-negative) Coulomb energies calculated by the octree-based method compared to the DSF method for distances between the cation and droplet surface of less than 15 Å, as shown in Fig. 7(b). The one-to-

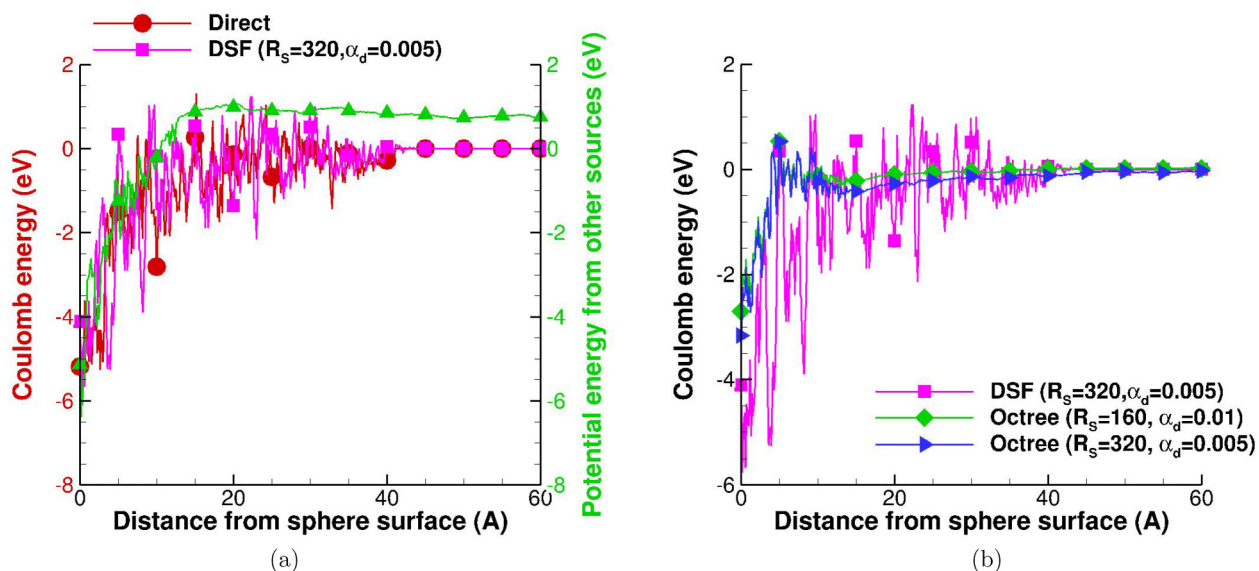


FIG. 7. Comparison of Coulomb energy of the constrained cation with potential energy contribution from other sources shown in (a). Comparison of Coulomb energy of the constrained cation from damped octree-based Coulomb interaction model shown in (b).

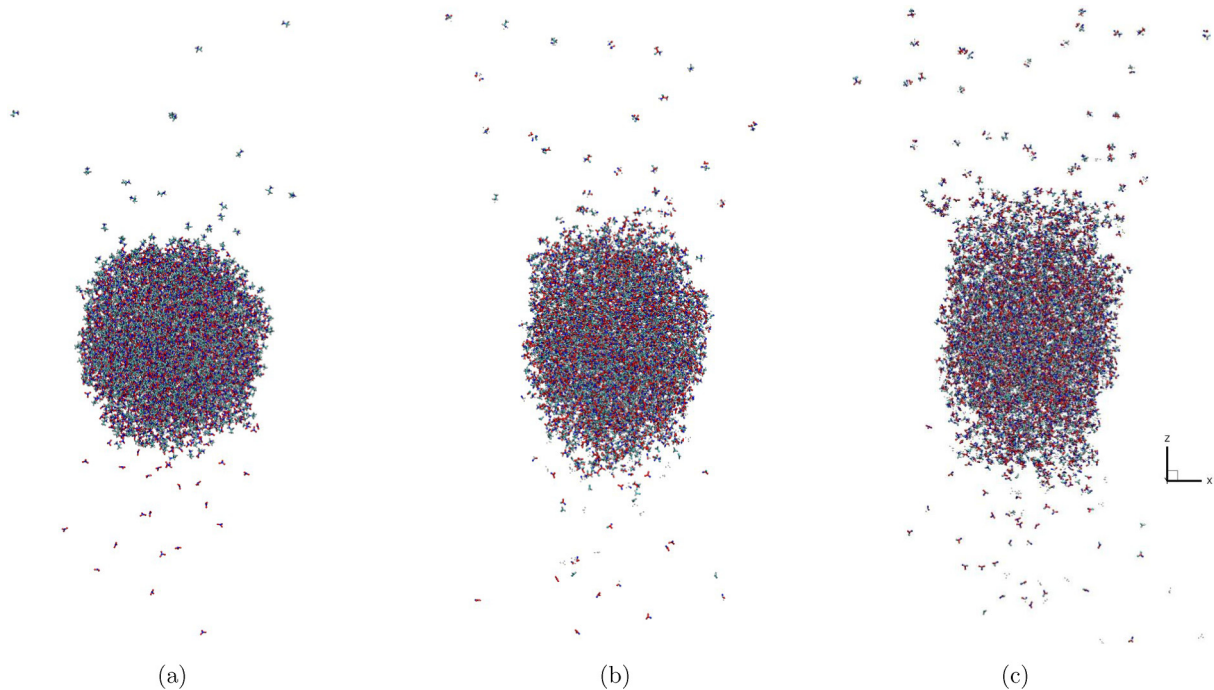


FIG. 8. Snapshots of the primary droplet simulation in the presence of an external electric field. This case is performed with damped octree-based Coulomb interaction method with $R_S = 320 \text{ \AA}$ and $\alpha_d = 0.005$. Droplet structure in (a), (b), and (c) is at a simulation time of 2.5, 5.0, and 7.5 ps, respectively.

one electrostatic interactions between all atoms also leads to noisier Coulomb energies for the DSF method compared to the results from the octree-based method. When the cation-droplet surface distance is more than 15 \AA , the Coulomb energies from the octree-based method and the DSF are in

reasonable agreement and the result from the octree-based Coulomb interaction method is markedly less noisy. For the cation-droplet surface distance greater than 15 \AA , the majority of the Coulomb interactions between the cation and primary droplet atomic partial charges in the octree-based Coulomb

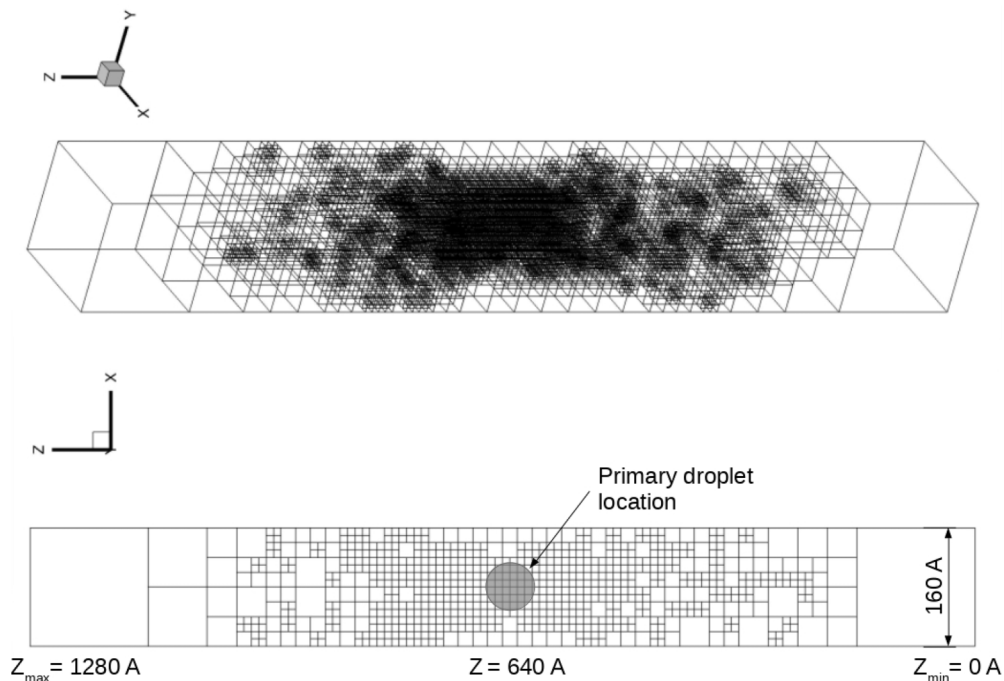


FIG. 9. Octree structure generated by the damped octree-based method for the droplet simulation in the presence of external electric field at 7.5 ps [see Fig. 8(c)]. Top and bottom: isometric and front view. The smallest leaves are of size equal to $R_{\text{inner}} = 10 \text{ \AA}$.

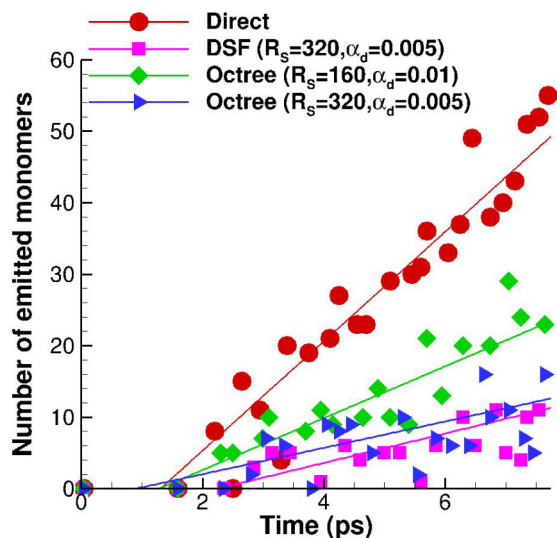
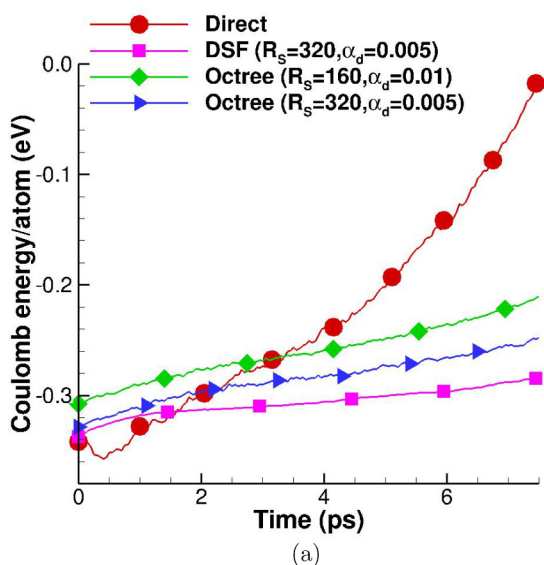


FIG. 10. Comparison of number of secondary monomers emitted from the primary droplet in the presence of external electric field.

method is calculated using charge coarsening, which leads to a smoother Coulomb energy. The difference between the Coulomb energy from the octree-based and the DSF method at distances less than 15 \AA does not cause significant differences in the total Coulomb energy of the system, as seen in the good agreement shown previously in Fig. 5(b). It is also worth noting that the intramolecular potential contributions from other sources, such as the covalent bonds, angle, and dihedral terms, are more dominant than the Coulomb energy for a single cation beyond a 15 \AA distance from the primary droplet, as shown in Fig. 7(a). However, for a system of many charged particles in the presence of external fields, as is the case for electrosprays, Coulomb interactions do exert considerable influence on the emission characteristics, as discussed next.



IV. MD SIMULATIONS WITH THE OCTREE-BASED COULOMB METHOD IN AN EXTERNAL ELECTRIC FIELD

Coulomb interactions are significant in dense charge systems especially in the presence of an external electric field which inputs energy into the system to overcome cohesive Coulomb interactions between ion pairs. To study the ability of the octree Coulomb method to model such systems two types of cases are considered in this section. First, the primary droplet geometry considered in the previous section is now simulated assuming external radial and normal electric field strengths of 0.05 and 0.5 V/\AA , respectively. These values reflect the field strengths that were observed near the electrospray capillary exit by solving Laplace's equation with an extrusion potential of -60 V and the *tip* boundary condition, as discussed in our previous work [47].

In a second, larger simulation, $19,810$ ion pairs of EAN were placed inside a capillary formed by placing $17,115$ platinum atoms as a hollow cylinder open on both ends, forming a radius of 59 \AA and a height of 290 \AA . The capillary was formed by placing $17,115$ platinum atoms as a hollow cylinder, open on both ends. The EAN ion pairs were randomly placed inside the volume of the cylinder formed by the platinum atoms. Similarly to the primary droplet simulations, the capillary filled with the EAN ion pairs was also potential energy minimized to remove spurious atom-bond overlaps. This was followed by 250 ps of a canonical ensemble simulation to equilibrate the IL within the capillary at 295 K . The extrusion simulation were then performed by superimposing the external electric field calculated using Laplace's equation for an extrusion potential of -60 V for the *tip* boundary condition [12]. The EAN ion pairs were ejected from the capillary using a moving potential wall to generate a mass flow rate of $2.50 \times 10^{-12} \text{ kg/s}$. The domain size for the extrusion simulation was $320 \times 320 \times 1280 \text{ \AA}$, such that the bottom of the capillary was placed normal to the x - y plane at

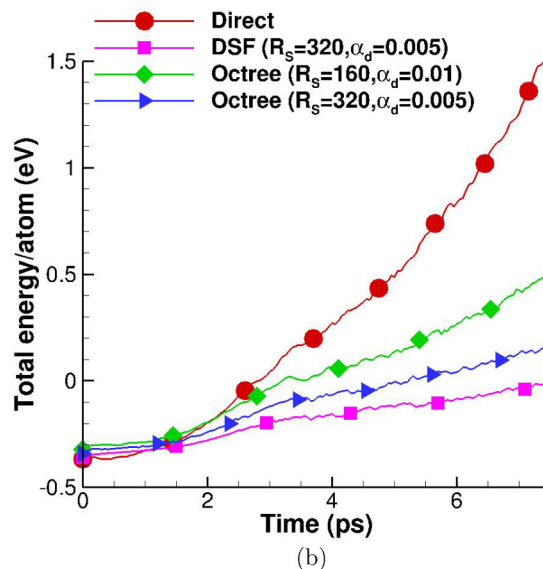


FIG. 11. Comparison of Coulomb energy and total energy per atom of the primary droplet in the presence of external electric field shown in (a) and (b), respectively.

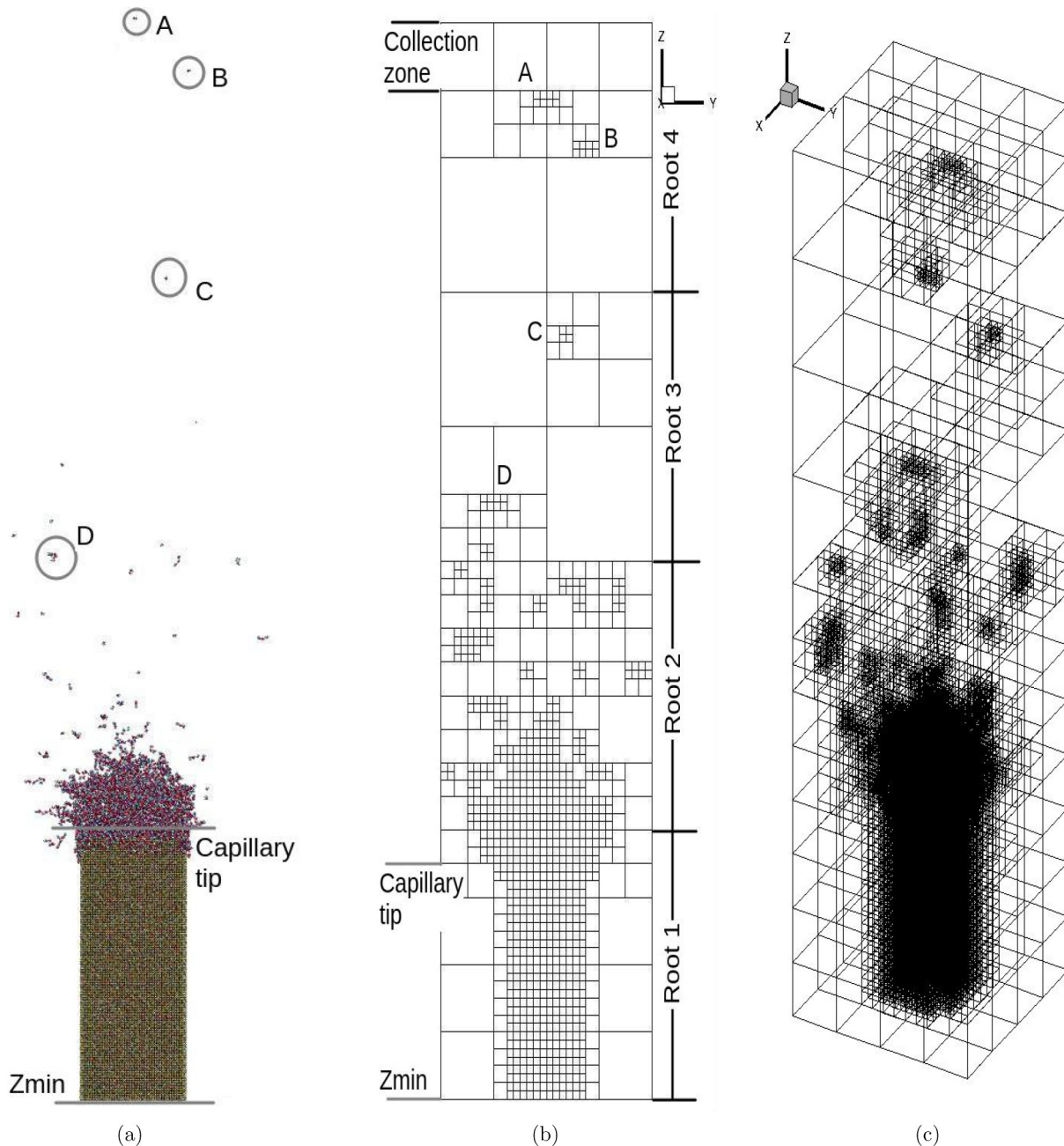


FIG. 12. Snapshot of atomic partial charge positions at 30 ps (a) for the capillary electrospay simulation performed with damped octree-based Coulomb interaction method, and front (b) and isometric (c) views of the generated corresponding octree structure. Radius of the capillary is 59 Å.

$z = 0$. To quantify ion emission from the extrusion simulations, emission currents are obtained by tallying the emitted ions at the collection zone, which is located 1000 Å away from the tip of the capillary. The collection zone starts in the x - y plane at $z = 1270$ Å and continues up to $z = 1280$ Å. The lower plane of the collection zone is known as the extrusion plane. During the simulations, emitted ion species are tallied in the collection zone to calculate the emission currents. The height of the collection zone is deliberately set at 10 Å, such that it is adequate to tally the emission but small enough to avoid double counting which may occur before the emitted ion species are removed from the domain.

A. Droplet evolution in the presence of an external field

Snapshots from the droplet evolution simulation for the octree-based Coulomb interaction model with $R_S = 320$ Å and $\alpha_d = 0.005$ are shown in Fig. 8. After 2.5 ps of simulation time, the primary droplet starts emitting secondary monomers (cations) toward the positive Z direction and anions toward the negative Z direction, as shown in Fig. 8(a). Unlike the spherical shape held by the droplet at 2.5 ps, significant deformation of the primary droplet can be observed after 5.0 ps, which is accompanied by a higher emission of secondary ions, as shown in Fig. 8(b). The primary droplet loses its shape and is on the verge of complete fragmentation after 7.5 ps

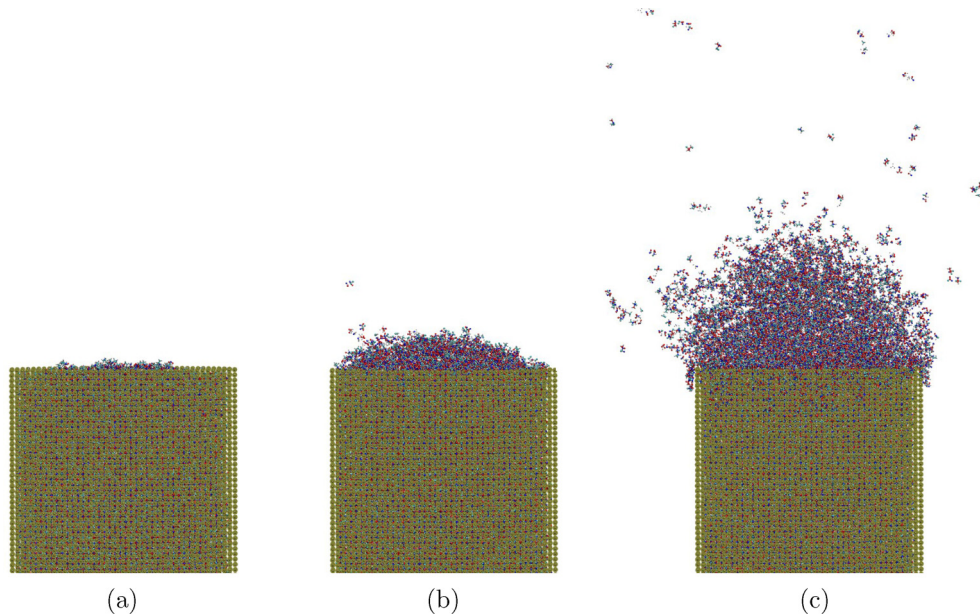


FIG. 13. Snapshots of the Taylor's cone formation during the capillary electrospay simulation. This case is performed with damped octree-based Coulomb interaction method with $R_S = 320 \text{ \AA}$, intraleaf Coulomb $\alpha_d = 0.005$, and interleaf Coulomb $\alpha_d = 0.1$. The radius of the cylinder is 59 \AA . Snapshots at simulation times of 2.5, 25, and 35 ps are shown in (a), (b), and (c), respectively.

in the presence of the external fields, as shown in Fig. 8(c). The particular arrangement of atoms shown in Fig. 8(c) is a simulation domain with a discrete distribution of charged particles, which is where the octree-based Coulomb method performs especially well. The octree generated for this simulation domain at 7.5 ps is shown in Fig. 9. It can be observed that the octree leaves (cells) are more refined near the center region with higher charge density and becomes coarser near the Z_{\min} and Z_{\max} boundaries.

A comparison of a linear curve fit obtained for the number of monomers emitted during the simulation for the different Coulomb models is shown in Fig. 10. For all Coulomb models, it was observed that only monomers were emitted during the simulation. It is evident that the number of monomers emitted by the direct Coulomb method is markedly higher compared to that from the DSF and octree-based simulations, even though, in the absence of any external fields, the Coulomb interactions calculated by all three methods are in relative agreement of about 4.0 %, as discussed in Sec. III B. When the first monomer is emitted, the limited Coulomb cut-off used by the direct Coulomb method restricts the Coulomb force that is exerted by the ion pair on the droplet beyond the cut-off distance resulting in a higher emission rate predicted by the direct Coulomb method. In contrast, for the DSF model, a much larger shift radius of $R_S = 320 \text{ \AA}$ and, consequently, a much smaller dampening parameter of $\alpha_d = 0.005$ increases the number of Coulomb interactions between ion pairs in the droplet as it fragments in the electric field compared to the direct method. This, in turn, lowers the DSF emission rate compared to that of the DC method. The strengths of the octree method become apparent during the dynamic evolution of the droplet in the presence of an external electric field. For the same R_S and α_d , the emission rate for the octree-based method is slightly higher compared to the DSF method because of its charge coarsening. However,

the use of charge coarsening is justified by the fact that the octree-based simulation is computationally two times faster compared to the DSF method and provides considerably good agreement. Predictably, when the shift radius, R_S , is lowered to 160 \AA , the octree-based emission rate is higher.

As shown previously in Fig. 5(a), the direct Coulomb method generates the most negative or strongest cohesion in the absence of an external electric field. However, when the electric field is applied, the Coulomb interactions calculated using the direct Coulomb method rapidly start decreasing (less negative), faster than other methods, as shown in Fig. 11(a). These trends occur because more stable Coulomb energies are calculated over longer distances with the DSF and the octree-based method that limit the rise (decrease) of Coulomb energy. This is also reflected in the gradual increase in the total energy (sum of potential and kinetic) of the system, shown in Fig. 11(b). The octree-based Coulomb model provides the ability to account for long-range Coulomb forces that counteract the acceleration of monomers extracted by the external electric field. This limits the kinetic energy gained by the secondary in-pair emissions, thus slowing the increase in the kinetic energy of the system.

B. Capillary electrospay at $2.5 \times 10^{-12} \text{ kg/s}$

Having validated the performance of the octree-based Coulomb method for the droplet geometry in the presence of an electric field, simulations of the electrospay process are performed to study the formation of Taylor's cone and the extrusion process. The capillary simulations contain a comparatively large number of atoms (314 265) and, therefore, 512 processors were used to perform the capillary electrospay simulations. Although the DSF and the octree-based methods are demonstratively superior in modeling emission from the IL droplet in the presence of an external electric field, the

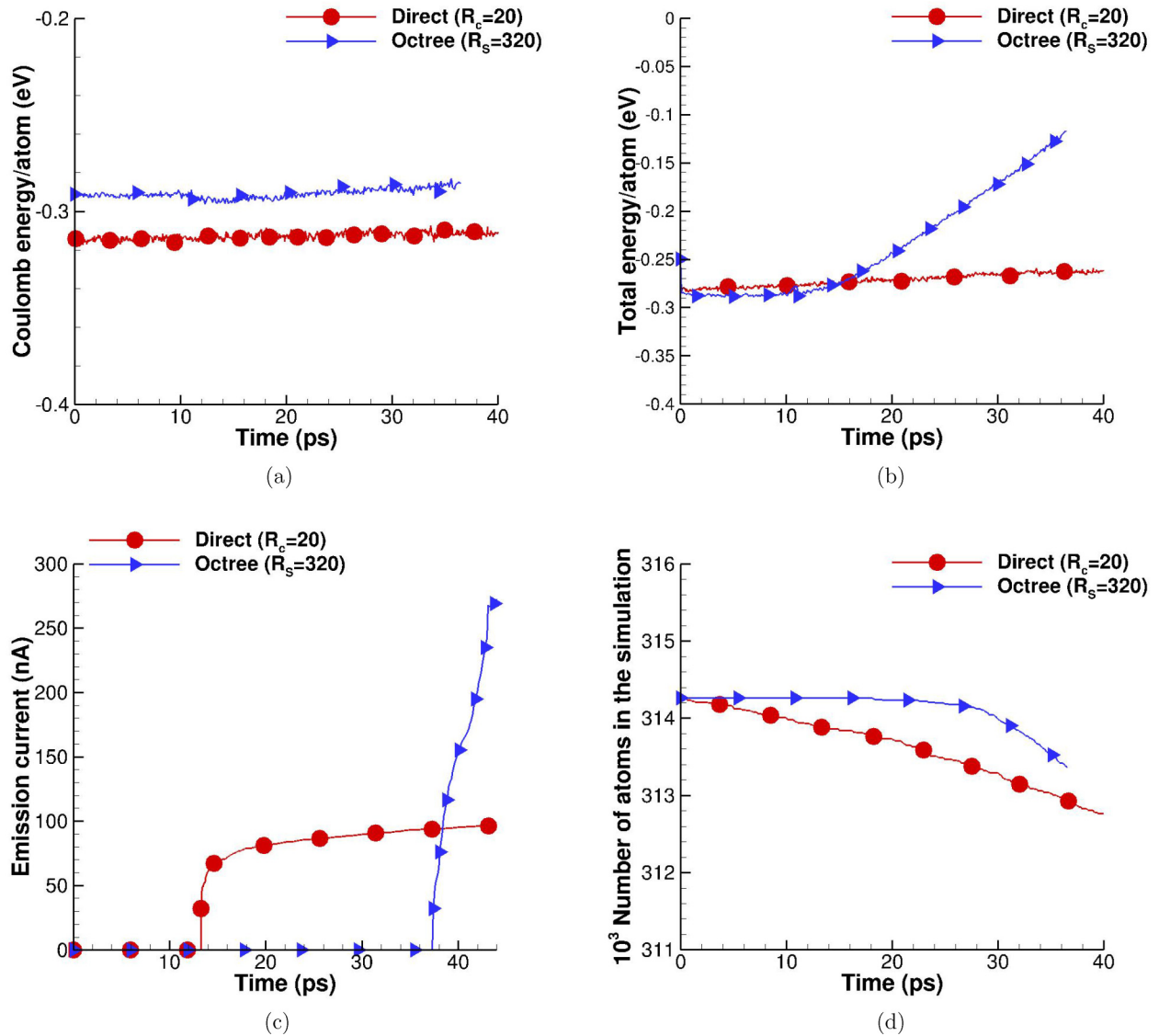


FIG. 14. Comparison of Coulomb (a), total energy per atom (b), emission currents (c), and number of atoms present in the simulation (d) during the capillary extrusion simulations. Figures 14(a), 14(b), and 14(d) use MD data collected over the entire domain and include both anions and cations.

former cannot be used for the capillary geometry since the computational cost required for such a simulation would be prohibitively high for an $R_S = 320$ Å. Therefore, to compare the emission rate and currents obtained from the octree-based Coulomb model, simulations were also performed using the direct Coulomb method with a comparatively smaller cut-off radius of 20 Å, because even a 40 Å value would be untenable. When using the octree-based method, initial computations with a shift radius of $R_S = 320$ Å and $\alpha_d = 0.005$ indicated kinetic heating of the ionic liquid within the capillary due to thermal motion of the atoms as they move through a distance greater than the shift radius. While the shift radius of 320 Å and an associated dampening parameter of 0.005 provided converged Coulomb energies for the droplet geometry, the columnar arrangement of IL bulk in the capillary gives rise to highly nonsymmetric interactions between ion pairs within the shift radius leading to spurious kinetic energy gains for the smaller dampening parameter. Therefore, the

dampening parameter was increased to $\alpha_d = 0.1$ only for the interleaf Coulomb interactions, but $\alpha_d = 0.005$ was used for the intraleaf Coulomb component. The shift radius was unchanged for both octree components. The octree structure for a snapshot of atomic partial charge positions at 30 ps is shown in Fig. 12. At 30 ps, the Taylor's cone structure is almost fully formed and, as shown in Fig. 12(a), ion-species emission can be seen occurring from the sides as well as the tip of the Taylor cone. Monomers A–C and dimer D can be seen to be moving toward the collection zone. As shown in Fig. 12(b), the octree grid is refined in the regions containing these ion species. The three-dimensional isometric view of the octree structure generated for the atomic partial charge positions at 30 ps is shown in Fig. 12(c).

Snapshots of the Taylor's cone formation from the MD simulation using the octree-based method are shown in Fig. 13. The snapshot in Fig. 13(a), obtained at 2.5 ps, shows ion pairs creating the upper meniscus of the IL inside the

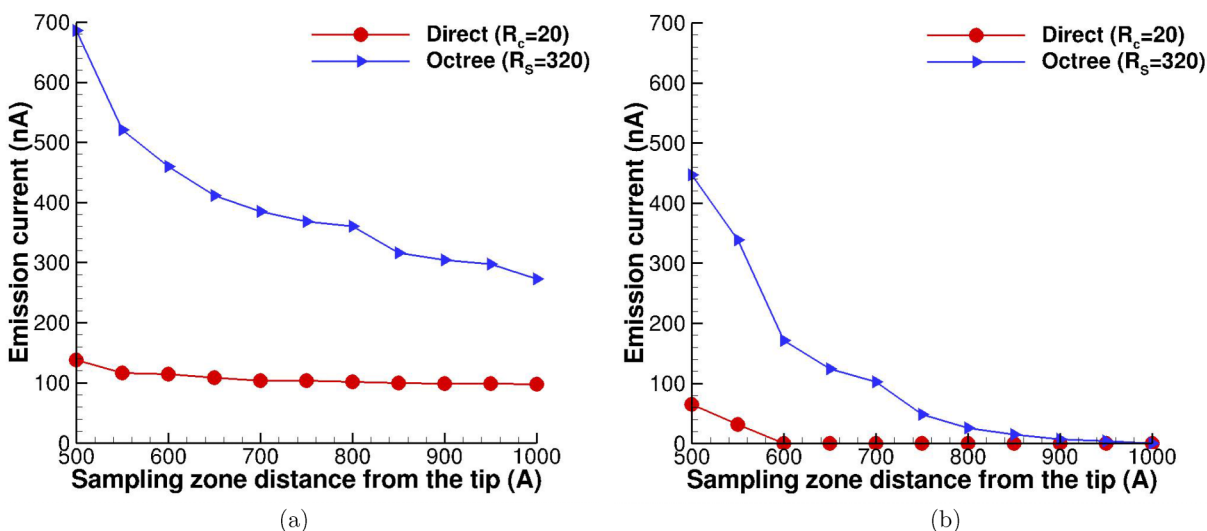


FIG. 15. Comparison of the cation monomer (a) and dimer (b) emission currents as a function of distance from the capillary tip, obtained from the octree-based and direct Coulomb methods for 2000 frames after 20 ps simulation time.

capillary within its tip. At 25 ps, the external electric field affects the shape of the bulk structure of IL pushed out of the capillary, which initiates the formation of the Taylor's cone, as shown in Fig. 13(b). The fully formed Taylor's cone is seen in Fig. 13(c) at the tip of the capillary at 35 ps. The process of formation of the Taylor's cone is similar for both the direct and octree-based Coulomb methods. However, the slightly weaker Coulomb energies generated due to dampening in the octree-based method causes the Taylor's cone structure to form approximately 15 ps earlier compared to the direct Coulomb method.

Similarly to the droplet evolution case, the Coulomb energy per atom of the system from the octree-based method is within 3% agreement of that obtained from the direct Coulomb method, as shown in Fig. 14(a). The charge coarsening coupled with heavier dampening for interleaf terms ($\alpha_d = 0.1$) generates a system with marginally weaker Coulomb interactions but this weakening is small and, in fact, predicts somewhat slower ion emission and atom loss rate, as seen in Figs. 14(c) and 14(d), respectively. The total energy (sum of potential and kinetic energies) comparison, shown in Fig. 14(b), reveals significant differences between the octree-based and the direct Coulomb methods. During the initial stages of the Taylor's cone formation, there is a steady growth in the total energy for both the methods. Since the Coulomb energies of both the simulations are relatively constant, as shown in Fig. 14(a), the rise in the total energy can be attributed primarily to the kinetic energy gain. In the octree-based method, as the Taylor's cone is being formed, more accurate representation of long-range Coulomb interactions predicts the emission of larger ion species, such as dimers and trimers as the Taylor's cone is forming, which leads to a rise in the total energy of the system beyond the first 15 ps.

Similarly to the droplet emission case, when the ion species are tallied at the collection zone, only monomer emission is observed from both the simulations. Since the ion emission is not continuous, emission currents are presented as

cumulative moving averages for the two methods in Fig. 14(c). Consistent with the gain in kinetic energy of the system, monomer emission current from the octree-based method is higher compared to that from the direct method. However, the time of first emission is delayed for the octree-based Coulomb interaction method. Even though the emission currents from the octree-based simulation is higher, the long-range Coulomb interactions provide stability to the Taylor's cone structure, ensuring that the emission of ion species occurs toward the extrusion zone and not toward the sides. This is also reflected in the rate of loss of atoms from the simulation domain during the Taylor's cone formation. As shown in Fig. 14(d), there is a continuous loss of atoms from the domain when the direct Coulomb method is used. In comparison, the loss of atoms during the formation of

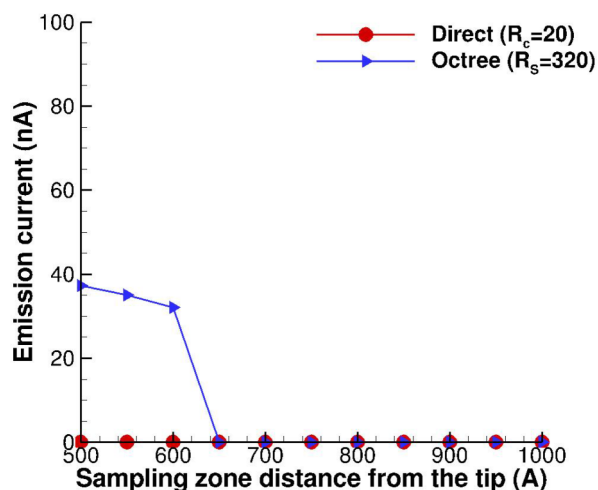


FIG. 16. Comparison of the cation trimer emission currents as a function of distance from the capillary tip, obtained from the octree-based and direct Coulomb methods for 2000 frames after 20-ps simulation time.

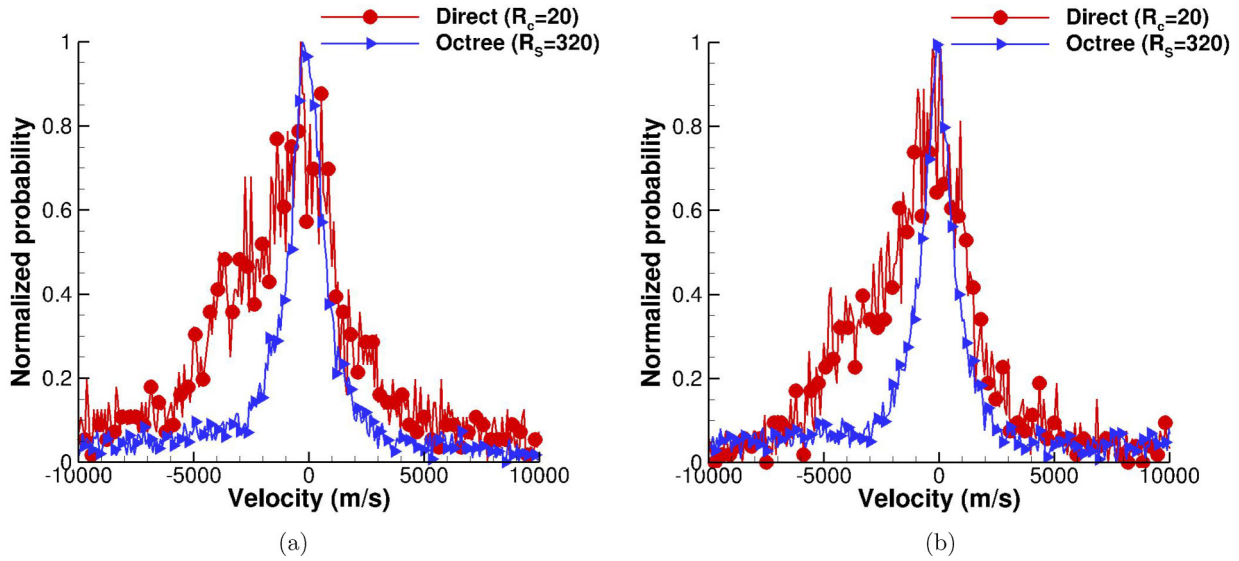


FIG. 17. Comparison of the normalized X (a) and Y (b) velocity distribution functions of the atomic partial charges emitted at the tip of the capillary, obtained from the octree-based and direct Coulomb methods for cations after 20 ps for 2000 time frames.

the Taylor's cone, prior to 30 ps, is significantly lower for the octree-based method, even though the Coulomb energy it predicts is weaker compared to the direct method, as shown in Fig. 14(a).

There are quantifiable differences between the octree-based Coulomb and direct Coulomb simulations in terms of emission species and currents. Even though the Coulomb energy of the system predicted by the direct Coulomb method is more negative compared to the octree-based method, the limited region within which the Coulomb interactions are calculated for the direct Coulomb method leads to more emission of smaller ions rather than larger species. Also, only monomers were observed in the collection zone since any larger ion species that were emitted from the Taylor's cone underwent further fragmentation due to energy obtained from the external electric field while moving toward the collection zone. To better understand the nature of emissions from the Taylor cone, instead of only tallying ion species at the fixed collection zone 1000 Å away from the tip of the Taylor's cone, the ion species are tallied every 50 Å from the capillary tip. Comparisons of the monomer, dimer, and trimer emissions as a function of distance from the capillary tip, for the two simulations, are shown in Figs. 15(a), 15(b) and 16, respectively. While no species larger than monomers were observed from the direct Coulomb simulation at any distance from the capillary tip, significant emission currents from the dimer and trimer were observed closer to the capillary tip from the octree-based simulation, as shown in Figs. 15(b) and 16, respectively. From our previous simulations [47], it was observed that larger ion species are emitted only from a well-formed, coherent Taylor's cone. Thus, it can be concluded that the octree-based Coulomb model promotes the formation of a more coherent Taylor cone structure compared to the direct Coulomb method and, as a consequence, the latter method does not predict the emission of larger ion species.

The lower emission current coupled with the higher loss of ion pairs predicted by the direct Coulomb model [see Figs. 14(c) and 14(d), respectively] suggests that a majority

of ion pairs emitted from the capillary do not contribute to the emission currents tallied at the collection zone. These are lost or wasted when they leave from the lateral boundaries due to sideways or radial emission since they do not contribute to the emission currents after the Taylor cone is formed. The Taylor's cone structure is also weaker and hence allows a higher number of ion pairs to escape, leading to significant, albeit a wasteful, loss of ion pairs from the domain. This was measured by comparing the velocity distribution functions for all cations emitted from the capillary for both the simulations. A comparison of the X and Y lateral velocity components shows that the distribution is narrower for cations emitted from the octree-based simulation, as shown in Figs. 17(a) and 17(b). This indicates that when the direct Coulomb method

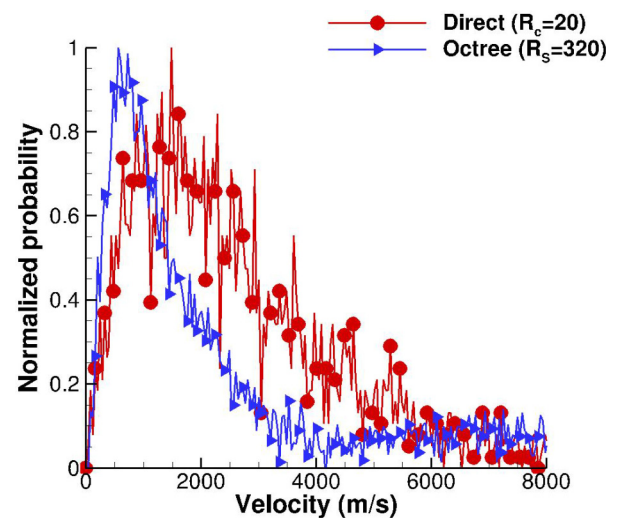


FIG. 18. Comparison of the normalized Z (c) velocity distribution functions of the atomic partial charges emitted at the tip of the capillary, obtained from the octree-based and direct Coulomb methods for cations after 20 ps for 2000 time frames.

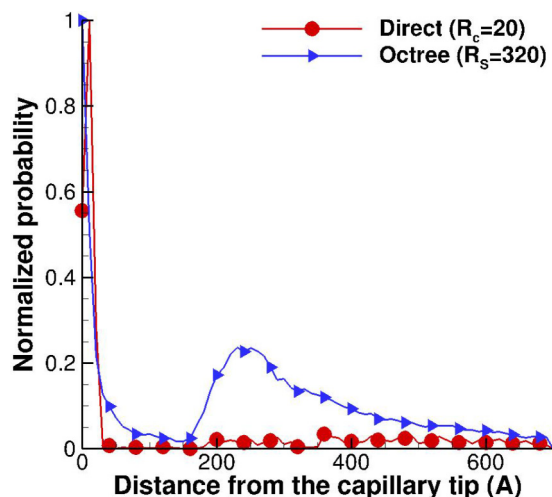


FIG. 19. Comparison of the normalized emission probability distribution functions of both cations and anions emitted between 20 and 45 ps, obtained from the octree-based and direct Coulomb methods. Capillary tip is located at $z = 290 \text{ \AA}$.

is used, ion pairs are emitted with higher lateral velocities compared to that observed when the octree-based method is used. Another significant difference between the two methods can be noted from the distribution of the axial (Z component of) velocity. As shown in Fig. 18, the distribution from the octree-based simulation is not only comparatively narrower but also the peak of the distribution is located at a lower axial velocity compared to that observed from the direct Coulomb method. This is again indicative of heavier cations such as dimers and trimers that are emitted when the octree-based Coulomb method is used.

While the Taylor's cone was observed in both set of simulations, the stability provided to this structure due to long-range Coulomb interactions by the octree-based Coulomb method generates more focused, concentrated emission. This was analyzed by generating a probability distribution of distance from the capillary tip at which the ions leave the domain between 20 and 45 ps during the simulation, representing the time during which the Taylor's cone is partially to fully formed. As shown in Fig. 19, the normalized probability distributions from the two methods are considerably different. The peak of both distributions lie within 100 \AA from the capillary tip and is composed of monomer anions that cannot travel toward the collection zone because the applied electric field is positive. That is, anions leave the domain from the lateral boundaries at distances less than 100 \AA from the capillary tip. The secondary peak observed from the octree-based simulation represents the distance away from the capillary tip at which a large fraction of cations leave the domain. The wider velocity distribution from the direct Coulomb simulation indicates that the cone emission is isotropic and the majority of the ions emitted from the capillary are lost laterally, soon after they are emitted.

V. CONCLUSIONS

In this work, we have used a modified Barnes-Hut algorithm to develop an octree-based Coulomb interaction model targeted toward simulations of ILs in the presence of

external electric fields and sparse, nonperiodic domains. The Coulomb interactions are subdivided into intra- and interleaf Coulomb interactions based on the Bjerrum length criterion, thus associating the Coulomb cut-off criterion with a physical electrochemical property of the simulated IL. The energy conservation validation of the octree-based method showed that attention must be paid to the selection of the shift radius and dampening parameters to avoid spurious gains in the kinetic energy of the system. To obtain agreement with the direct Coulomb and DSF method Coulomb energies, the octree method simulations were performed with $R_S = 320 \text{ \AA}$ and $\alpha_d = 0.005$. Using a smaller shift radius and, consequently, a larger dampening parameter would lead to weaker Coulomb energies of the system. It should be noted that the selection of R_S and α_d was based on the characteristic dimensions of the simulation, such as the radius of the primary droplet and the length of the capillary. It is advisable to use the largest characteristic length present in the simulation as a shift radius when employing the octree-based Coulomb interaction method to avoid the need to run simulations to estimate its value. The use of the octree-based Coulomb interaction model in the absence of an electric field does not change the physical properties of the simulated ILs, such as the radial density function.

While the Coulomb and total energy of the system obtained from the direct, DSF, and the octree-based methods are in reasonable agreement in the absence of external electric fields, the differences are significant between the direct and the octree-based method in the presence of an external electric field. For the droplet evolution test case, the ability to account for Coulomb interactions over longer distances limited the emission of ions when the octree-based Coulomb interaction model was used, even though the Coulomb energies of the entire system are weaker (less-negative) compared to that predicted by the direct Coulomb method. For the same droplet geometry, the octree-based Coulomb method was found to be twice as fast compared to the DSF method, while providing a good agreement in Coulomb energies and ion emission rates.

For the capillary-based simulations, the long-range Coulomb interactions captured by the interleaf Coulomb term in the octree-based method reduces the Taylor cone formation time compared to the direct Coulomb model. Furthermore, emission of larger species, such as dimers and trimers, was observed only from the simulation performed with the octree-based Coulomb interaction model. The lack of long-range interactions leads to larger tangential or cross-stream emission of ions and subsequent loss of atoms when the direct Coulomb method is used to model extrusion from the capillary geometry. This resulted in a significantly lower emission current compared to that obtained from the octree-based Coulomb interaction model. Finally, it was shown that the emission of ions from the Taylor's cone was into a smaller angle when the octree-based method was used for the capillary extrusion case.

ACKNOWLEDGMENT

Funding for this work was provided by the Air Force Office of Scientific Research (AFOSR) through Dr. Mittat Birkan under Grant No. AF FA9550-16-1-0193. We are thankful to XSEDE TACC for providing us with the vital computational resources on their STAMPEDE2 cluster.

- [1] W. Deng, C. M. Waits, and A. Gomez, Digital electrospray for controlled deposition, *Rev. Sci. Instrum.* **81**, 035114 (2010).
- [2] A. Jaworek, Electrospray droplet sources for thin film deposition, *J. Mater. Sci.* **42**, 266 (2007).
- [3] L. Swanson, Liquid metal ion sources: Mechanism and applications, *Nucl. Instrum. Methods Phys. Res.* **218**, 347 (1983).
- [4] R. Clampitt, Advances in molten metal field ion sources, *Nucl. Instrum. Methods Phys. Res.* **189**, 111 (1981).
- [5] J. B. Fenn, M. Mann, C. K. Meng, S. F. Wong, and C. M. Whitehouse, Electrospray ionization for mass spectrometry of large biomolecules, *Science* **246**, 64 (1989).
- [6] M. Gamero-Castano and V. Hruby, Electrospray as a source of nanoparticles for efficient colloid thrusters, *J. Propul. Power* **17**, 977 (2001).
- [7] V. Hruby, M. Gamero-Castano, D. Spence, C. Gasdaska, N. Demmons, R. McCormick, P. Falkos, J. Young, and W. Connolly, Colloid thrusters for the new millennium, st7 drs mission, in *2004 IEEE Aerospace Conference Proceedings (IEEE Cat. No.04TH8720)* (IEEE, Big Sky, MT, USA, 2004), p. 213, Vol. 1.
- [8] B. Donius and J. L. Rovey, Ionic liquid dual-mode spacecraft propulsion assessment, *J. Spacecr. Rockets* **48**, 110 (2011).
- [9] B. D. Prince, P. Tirupathi, R. J. Bemish, Y.-H. Chiu, and E. J. Maginn, Molecular dynamics simulations of 1-ethyl-3-methylimidazolium bis[(trifluoromethyl)sulfonyl]imide clusters and nanodrops, *J. Phys. Chem. A* **119**, 352 (2015).
- [10] G. I. Taylor, Disintegration of water droplets in an electric field, *Proc. Roy. Soc. A* **280**, 383 (1964).
- [11] A. Borner and D. A. Levin, Use of advanced particle methods, Modeling space propulsion and its supersonic expansions, Ph.D. Dissertations, PSU, 2014.
- [12] N. A. Mehta and D. A. Levin, Sensitivity of electrospray molecular dynamics simulations to long-range coulomb interaction models, *Phys. Rev. E* **97**, 033306 (2018).
- [13] M. Allen and D. Tildesley, *Computer Simulation of Liquids* (Clarendon Press, London, 1989).
- [14] C. J. Fennell and J. D. Gezelter, Is the ewald summation still necessary? Pairwise alternatives to the accepted standard for long-range electrostatics, *J. Chem. Phys.* **124**, 234104 (2006).
- [15] R. W. Hockney and J. W. Eastwood, *Computer Simulations Using Particles* (CRC Press, Boca Raton, FL, 1988).
- [16] J. A. Barnes and H. Piet, A hierarchical $O(N \log N)$ force-calculation algorithm, *Nature* **324**, 446 (1986).
- [17] T. Hamada, K. Nitadori, K. Benkrid, Y. Ohno, G. Morimoto, T. Masada, Y. Shibata, K. Oguri, and M. Taiji, A novel multiple-walk parallel algorithm for the barnes-hut treecode on gpus – toward cost effective, high performance n-body simulation, *Comput. Sci. Res. Dev.* **24**, 21 (2009).
- [18] L. Greengard and V. Rokhlin, A new version of the fast multipole method for the laplace equation in three dimensions, *Acta Numer.* **6**, 229 (1997).
- [19] J. Kurzak and B. M. Pettitt, Fast multipole methods for particle dynamics, *Molec. Simul.* **32**, 775 (2006).
- [20] G. Mathias, B. Egwolf, M. Nonella, and P. Tavan, A fast multipole method combined with a reaction field for long-range electrostatics in molecular dynamics simulations: The effects of truncation on the properties of water, *J. Chem. Phys.* **118**, 10847 (2003).
- [21] S. Aluru, J. Gustafson, G. M. Prabhu, and F. E. Sevilgen, Distribution independent hierarchical algorithms for the n body problem, *J. Supercomput.* **12**, 303 (1998).
- [22] R. Yokota and L. A. Barba, A tuned and scalable fast multipole method as a preeminent algorithm for exascale systems, *Int. J. High Perf. Comput. Appl.* **26**, 337 (2012).
- [23] N. H. Chau, Parallelization of the fast multipole method for molecular dynamics simulations on multicore computers, in *Advanced Computational Methods for Knowledge Engineering*, edited by N. T. Nguyen, T. van Do, and H. A. le Thi (Springer, Heidelberg, 2013), pp. 209–224.
- [24] L. Greengard, The numerical solution of the n-body problem, *Comput. Phys.* **4**, 142 (1990).
- [25] F. Zhao and S. Johnsson, The parallel multipole method on the connection machine, *SIAM J. Sci. Stat. Comput.* **12**, 1420 (1991).
- [26] J. Kurzak and B. M. Pettitt, Communications overlapping in fast multipole particle dynamics methods, *J. Comput. Phys.* **203**, 731 (2005).
- [27] J. Kurzak and B. M. Pettitt, Massively parallel implementation of a fast multipole method for distributed memory machines, *J. Parallel Distrib. Comput.* **65**, 870 (2005).
- [28] S. F. Frisken and R. N. Perry, Simple and efficient traversal methods for quadrees and octrees, *J. Graph. Tools* **7**, 1 (2002).
- [29] R. Jambunathan and D. A. Levin, Chaos: An octree-based pic-dsmc code for modeling of electron kinetic properties in a plasma plume using mpi-cuda parallelization, *J. Comput. Phys.* **373**, 571 (2018).
- [30] S. Plimpton, Fast parallel algorithms for short-range molecular dynamics, *J. Comput. Phys.* **117**, 1 (1995).
- [31] R. Hayes, S. Imberti, G. G. Warr, and R. Atkin, Amphiphilicity determines nanostructure in protic ionic liquids, *Phys. Chem. Chem. Phys.* **13**, 3237 (2011).
- [32] P. Walden, Ueber die molekulargrosse und elektrische leitfähigkeit einiger geschmolzenen salze, *Bull. l'Acad. Imper. Sci. St.-Petersb.* **8**, 405 (1914).
- [33] H. Weingärtner, A. Knocks, W. Schrader, and U. Kaatze, Dielectric spectroscopy of the room temperature molten salt ethylammonium nitrate, *J. Phys. Chem. A* **105**, 8646 (2001).
- [34] Y. Umebayashi, W. L. Chung, T. Mitsugi, S. Fukud, M. Takeuchi, K. Fujii, T. Takamuku, R. Kanzaki, and S. Ishiguro, Liquid structure and the ion-ion interactions of ethylammonium nitrate ionic liquid studied by large angle x-ray scattering and molecular dynamics simulations, *J. Comput. Chem. Jpn.* **7**, 125 (2008).
- [35] N. A. Mehta and D. A. Levin, Comparison of two protic ionic liquid behaviors in the presence of an electric field using molecular dynamics, *J. Chem. Phys.* **147**, 234505 (2017).
- [36] G. Lenguito, J. F. de la Mora, and A. Gomez, Scaling up the power of an electrospray microthruster, *J. Micromech. Microeng.* **24**, 055003 (2014).
- [37] R. Alonso-Matilla, J. Fernández-García, H. Congdon, and J. Fernández de la Mora, Search for liquids electrospraying the smallest possible nanodrops in vacuo, *J. Appl. Phys.* **116**, 224504 (2014).
- [38] J. V. L. Beckers, C. P. Lowe, and S. W. De Leeuw, An iterative ppm method for simulating coulombic systems on distributed memory parallel computers, *Molec. Simul.* **20**, 369 (1998).
- [39] D. Wolf, P. Keblinski, S. R. Phillpot, and J. Eggebrecht, Exact method for the simulation of coulombic systems by spherically

- truncated, pairwise r^{-1} summation, *J. Chem. Phys.* **110**, 8254 (1999).
- [40] R. E. Jones and D. H. Templeton, Optimum atomic shape for bertaut series, *J. Chem. Phys.* **25**, 1062 (1956).
- [41] D. M. Heyes, Electrostatic potentials and fields in infinite point charge lattices, *J. Chem. Phys.* **74**, 1924 (1981).
- [42] M. J. Stevens, M. L. Falk, and M. O. Robbins, Interactions between charged spherical macroions, *J. Chem. Phys.* **104**, 5209 (1996).
- [43] M. Tamashiro, Y. Levin, and M. C. Barbosa, Debye–hückel–bjerrum theory for charged colloids, *Physica A* **258**, 341 (1998).
- [44] W. L. Jorgensen, D. S. Maxwell, and J. Tirado-Rives, Development and testing of the oplis all-atom force field on conformational energetics and properties of organic liquids, *J. Am. Chem. Soc.* **45**, 11225 (1996).
- [45] J. S. Hansen, T. B. Schröder, and J. C. Dyre, Simplistic coulomb forces in molecular dynamics: Comparing the wolf and shifted-force approximations, *J. Phys. Chem. B* **116**, 5738 (2012).
- [46] P. Demontis, S. Spanu, and G. B. Suffritti, Application of the wolf method for the evaluation of coulombic interactions to complex condensed matter systems: Aluminosilicates and water, *J. Chem. Phys.* **114**, 7980 (2001).
- [47] N. A. Mehta and D. A. Levin, Molecular dynamics electro-spray simulations of coarse-grained ethylammonium nitrate (EAN) and 1-ethyl-3-methylimidazolium tetrafluoroborate (EMIM-BF₄), *Aerospace* **5**, 1 (2018).